

# UC Davis

## UC Davis Electronic Theses and Dissertations

### Title

Modeling, Experimentation and Analysis of an Indirect Evaporative Cooler

### Permalink

<https://escholarship.org/uc/item/93d073t5>

### Author

Jha, Apoorva

### Publication Date

2022

Peer reviewed|Thesis/dissertation

Modeling, Experimentation and Analysis of an Indirect Evaporative Cooler

By

APOORVA JHA  
THESIS

Submitted in partial satisfaction of the requirements for the degree of

MASTER OF SCIENCE

in

Mechanical and Aerospace Engineering

in the

OFFICE OF GRADUATE STUDIES

of the

UNIVERSITY OF CALIFORNIA

DAVIS

Approved:

---

Vinod Narayanan

---

Paul Erickson

---

Benjamin Shaw

Committee in Charge

2022

## ACKNOWLEDGEMENTS

I would like to express my sincere gratitude towards all of them without whom this work would not have materialized.

I extend my sincere and heartfelt gratitude to my advisor and Committee Chair, Professor Vinod Narayanan for his invaluable guidance, painstaking supervision and the opportunity of being a part of his research group. When I faced a roadblock or had a query about my research or writing, Prof. Narayanan was always there to help. Despite his busy schedule, he would meticulously work with me and extend all the support I could have asked for. His course not only tempered my technical know-how but also gave me great insights to technical writing which is something I shall strive to carry forward throughout my career. His kindness and thoughtfulness were a constant source of encouragement through some of the rough times I faced. Even through the remote meetings, he always tried to create a conducive space for all his students to share, learn and contribute comfortably and I am so glad to be a part of it.

I thank Prof. Shaw and Prof. Erickson who generously took the time out of their busy schedule to review my work and give their valuable feedback. Their guidance has been instrumental in the completion of my work.

I am deeply grateful to David Vernon, Co-Director of Engineering at the Western Cooling Efficiency Center (WCEC), for making it possible for me to pursue my project at this esteemed institute and for his kind and valuable mentorship. I gratefully acknowledge WCEC and Lawrence Berkeley National Laboratory (LBNL) for extending financial support through my research work.

I am indebted to Robert McMurry, R&D engineer, WCEC for his relentless efforts and time in initiating me into the world of experimental work. He was always there to assist and entertain any

and every question I had with utmost patience. I was also fortunate to be mentored by Subhrajit Chakraborty, R&D engineer, WCEC during a crucial phase of my research work. I am deeply thankful to Subhrajit for leading the experimental works conducted at WCEC and to Robert for his assistance.

I wish to warmly thank Vishal Singh for his unwavering encouragement, much-needed critical remarks ,and for constantly pushing me out of my comfort zones. I also appreciate Emily Fricke for being a wonderful lab partner to work with during some of the toughest days and for happily offering support whenever I was in need. I am thankful to all my senior and fellow lab members for sharing their expertise and discussing their research works, from which I always learned a lot.

My acknowledgments would be incomplete without expressing profound gratitude for my parents, Dr. C.S. Jha and Dr. Himani, who have been my first teachers in all realms of life and for being my inspiration and guiding light. I am eternally grateful for their endless support and motivation throughout my journey even from miles away. I lovingly acknowledge my little sister, Anindya who has always been my strength, pushed me to excel and believed that I am always capable of more.

## ABSTRACT

IECs (Indirect Evaporative Coolers) have emerged as a promising cooling technology due to their lower energy consumption and carbon footprint, improved efficiency, and a zero GWP alternative by avoiding the usage of refrigerants. The purpose of this research is to assess the thermal performance of an HMX (Heat and Mass Exchanger) in the form of an IEC developed by Seeley International . Indirect evaporative coolers (IEC) cool the primary air without adding humidity to the indoor environment by using the latent heat of vaporization of water in the secondary air stream. By pre-cooling the secondary air stream before extracting heat in cross-flow with the primary air, the Maisotsenko Cycle (M-Cycle) design of an IEC has the ability to approach dew-point temperatures. A sectional mathematical model was developed by linking the heat and mass transfer equations in discretized control volumes and solved in Engineering Equation Solver (F-Chart Inc.). Results from the model were validated using experimental data from lab experiments for conditions with no condensation on the primary side. The simulation findings were found to be in good agreement with the experimental data, with an error of less than 10% in the primary exit temperatures and secondary outlet humidity ratios; and less than 8% in the secondary exit temperatures. The mean average errors (MAE) reported for the primary outlet temperatures, secondary outlet temperatures ,and humidity ratios were 0.78 °C, 1.22°C and 0.0007 respectively. A parametric study was also carried out to evaluate the effects of some factors on the performance of the IEC, namely air flow rates, primary and secondary side channel lengths and heights, separation plate thickness and plate conductivity. Results concluded that the maximum impact on the performance parameters (dew-point and wet-bulb effectiveness and heat transferred) was exhibited by primary side air flow rate, channel lengths and heights of both primary and secondary side. The study corroborates the potential of IECs as a feasible cooling device besides suggesting the optimum design parameters.

<b>TABLE OF CONTENTS</b>	
<b>ACKNOWLEDGEMENTS</b>	<b>2</b>
<b>ABSTRACT</b>	<b>4</b>
<b>LIST OF FIGURES</b>	<b>vi</b>
<b>LIST OF TABLES</b>	<b>vi</b>
<b>INTRODUCTION &amp; LITERATURE REVIEW</b>	<b>7</b>
<b>1.1 Evaporative cooling</b>	<b>8</b>
1.1.1 Direct Evaporative Cooling	8
1.1.2 Indirect Evaporative Cooling	10
<b>1.2 M-cycle IEC</b>	<b>11</b>
<b>1.3 HRV/ERV</b>	<b>13</b>
<b>1.4 Recent advances in indirect evaporative cooling</b>	<b>16</b>
<b>METHODOLOGY</b>	<b>30</b>
<b>2.1 Equipment Description</b>	<b>30</b>
<b>2.2 Test Matrix</b>	<b>33</b>
<b>2.3 Governing Equations</b>	<b>34</b>
2.3.1 Geometric Inputs	38
2.3.2 Equations	39
<b>RESULTS AND DISCUSSION</b>	<b>43</b>
<b>3.1 Model Validation with Experimental data</b>	<b>43</b>
<b>3.2 Parametric Study</b>	<b>47</b>
3.2.1 Primary air flow rate	48
3.2.2 Secondary air flow rate	49
3.2.3 Primary channel length	51
3.2.4 Secondary channel length	53
3.2.5 Primary channel height	55
3.2.6 Secondary channel height	57
3.2.7 Plate thickness	59
3.2.8 Plate conductivity	60
<b>CONCLUSION AND SCOPE FOR FUTURE WORK</b>	<b>63</b>
<b>NOMENCLATURE</b>	<b>65</b>
<b>REFERENCES</b>	<b>69</b>
<b>Appendix</b>	<b>77</b>

## LIST OF FIGURES

Figure 1: Direct evaporative cooler (a)Schematic (b)Psychrometric process [13]	9
Figure 2: Indirect evaporative cooler (a)Schematic (b)Psychrometric process [13]	10
Figure 3: A heat recovery system [57]	14
Figure 4: Working principle of a regenerative IEC equipment [13]	19
Figure 5: Schematic of the evaporative air cooler [43]	23
Figure 6: Coolerado HRV/ERV schematic (sketch provided by Seeley) with zoomed in view of single core in the HMX section [66]	31
Figure 7: Unit cell representation of HMX (Sketch provided by Seeley)	32
Figure 8: Exploded view of the HMX [66]	32
Figure 9: Segment for dry-wet numerical analysis (a) Control volume as a part of the unit cell inset (b)Flow parameters entering and leaving control volume	36
Figure 10: Air flow distribution in the channels for one half core (top view)	37
Figure 11: Comparison of model results with experimental data for Primary Outlet Temperature	43
Figure 12: Comparison of model results with experimental data for Secondary Outlet Temperature	44
Figure 13: Comparison of model results with experimental data for Secondary Humidity Ratio	44
Figure 14: Model vs experimental data validation for core 5 for primary side.	46
Figure 15: Model vs experimental data validation for core 5 for secondary side.	47
Figure 16: Effect of Primary airflow rate	49
Figure 17: Effect of Secondary air flow rate	51
Figure 18: Effect of Primary channel length	53
Figure 19: Effect of secondary channel length	55
Figure 20: Effect of Primary channel height	57
Figure 21: Effect of Secondary channel height	58
Figure 22 :Effect of plate thickness	60
Figure 20: Effect of plate conductivity	60

## LIST OF TABLES

Table 1: Experimental test points	33
Table 2: Test matrix for parametric analysis	34
Table 3: Geometric parameters of the IEC	38
Table 4: Flow inputs to the model	38

## INTRODUCTION & LITERATURE REVIEW

Conventional vapor-compression refrigeration systems have flourished in the market for residential and commercial comfort cooling. While they are the most frequently used air-conditioning systems, as evidenced by their 95 percent market dominance [1], they have some significant environmental disadvantages such as high carbon footprint, greenhouse gas emissions [2], and high energy consumption [3,4]. Because of the impending energy scarcity, rising energy costs, and recently acknowledged environmental problems, interest in evaporative cooling has resurfaced. Evaporative cooling is favorable due to its low specific energy consumption [5], defined as the energy consumed per unit mass of the product (cooled) air, lack of ecologically harmful refrigerants and its diverse applications such as agricultural greenhouse cooling [6], data center [7] cooling, and building cooling. Recently, some work has also been done to explore the use of evaporative cooling systems beyond the conventional human thermal comfort applications- such as in water desalination and agricultural storage [8,9]. The research group in [8] proposed a technology called the Dew Point Desalination (DPD). DPD, unlike other thermal technologies, did not employ thermal power to evaporate water, and instead relied on water evaporation as the driving force. The thermal energy required to start the dew point cooling process was supplied to the DPD system via air, and the air was transported through the subsequent phases using electric energy. The system operated on ambient air, and even if an external source of thermal energy was not required to run the DPD system, pre-heating the ambient air that entered the system could considerably improve the effectiveness of its operation. Evaporative cooling systems were tested across various climates and the findings were promising. Research findings conducted in Dublin and Milan, two European cities representing lower and higher location ends of the temperate climatic conditions suggested that conventional cooling methods could be eliminated and successfully replaced by evaporative



cooling methods for year-round cooling in Dublin and non-summer cooling in Milan [10]. The accomplishment of a low-temperature difference between the water exiting the cooling tower and the ambient WBT is a critical feature of evaporative cooling viability in temperate areas (the primary approach temperature, PAT). This is required to maintain a sufficient supply of cooling water, especially during the summer when ambient WBTs are high. This is exacerbated by the requirement in modern systems to use a heat exchanger to separate the tower water circuit from the building cooling circuit. As a result, the temperature difference between the water entering the heat exchanger and the ambient WBT becomes the critical design parameter (the secondary approach temperature, SAT). The study of meteorological data showed that the desirable WBT to maintain the required SAT was statistically available for 53.7% of the year in Milan and 88% of the year in Dublin (Milan being a southern European city). Experiments conducted in scorching weather of Khoozsetan showed a decrease of 16% in power consumption and a 55% increase in COP as opposed to conventional air conditioners [11]. Furthermore, evaporative-cooling systems will likely have lower running costs and may have a lower beginning cost than a comparable mechanical system [12].

## 1.1 Evaporative cooling

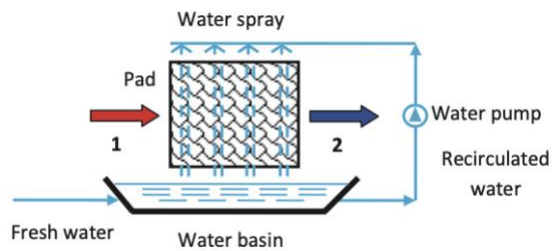
Evaporative cooling (EC) utilizes heat and mass transfer between the ambient air and the cooling liquid to achieve its cooling effect. Absorption of latent heat of vaporization leads to sensible cooling of the air stream through direct or indirect means.

### 1.1.1 Direct Evaporative Cooling

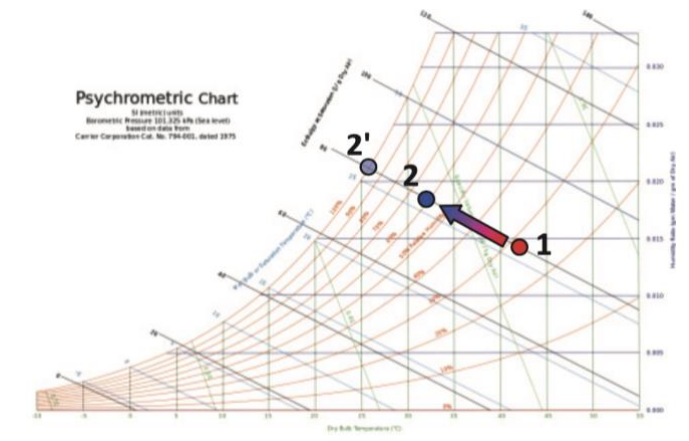
In air handling systems, this is the most prevalent type of evaporative cooling technique. Water sprayed into the incoming air stream raises the humidity and lowers the temperature. Heat is lost by the air stream as sensible heat and imparted to water as

latent heat. The working process is isenthalpic (Figure 1(b)), and the lowest achievable temperature is the saturation point, indicated by 2' in Figure 1(b).

The advantage of this approach is the simple construction of the equipment. Direct evaporative cooling has the drawback of being reliant on the incoming air's supply condition to provide adequate cooling. Also, humidification might be unfavorable for some specific applications.



(a)

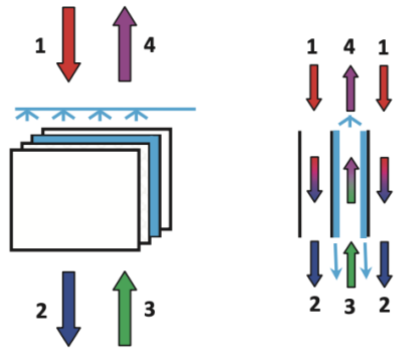


(b)

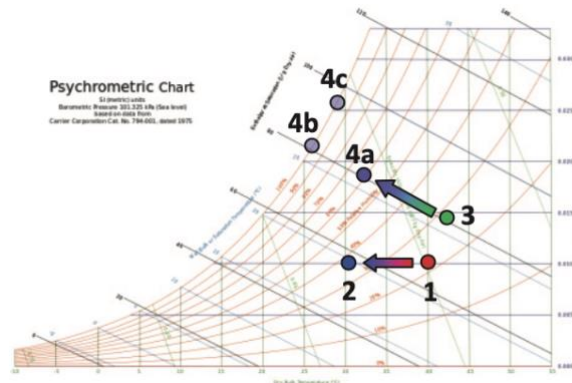
Figure 1: Direct evaporative cooler (a)Schematic (b)Psychrometric process [13]

### 1.1.2 Indirect Evaporative Cooling

Indirect evaporative cooling reduces air temperature without introducing moisture to the air, making it more appealing than direct evaporative cooling. In an indirect evaporative air cooler, primary (product) air flows over the dry side of a heat-exchanging wall while secondary (working) air goes over the opposite, wet side.



(a)



(b)

Figure 2: Indirect evaporative cooler (a)Schematic (b)Psychrometric process [13]

The heat transmitted across the surface between the dry and wet channels is absorbed as latent heat by the water, and a portion of the water is evaporated and incorporated

into the secondary air, thereby increasing the moisture content of this air. The primary air working process occurs at constant moisture, so long as the temperature does not drop below the dew point on this side.

If the secondary air arrives at saturation, the heat absorbed from the primary air is divided into latent heat absorbed by the water and sensible heat absorbed by the secondary air from this point on. As a result, the secondary air temperature at the outlet might be one of the following:

- i. Lower than secondary inlet wet bulb temperature when saturation has not been reached (point 4a as seen in Figure 2(b))
- ii. Equal to secondary inlet wet bulb temperature when saturation has been reached at outlet (point 4b as seen in Figure 2(b))
- iii. Higher than secondary inlet wet bulb when saturation is reached before the outlet. (point 4c as seen in Figure 2(b))

Since the inside air never interacts with the outside air, the interior atmosphere is less likely to be contaminated by external contaminants, making this a suitable technique for sensitive situations. The IEC's principal drawback is that the primary air-cooling process is constrained by the wet-bulb temperature of the secondary air at the input. Consequently, this device is also referred to as the wet-bulb IEC. [13]

## 1.2 M-cycle IEC

The Maisotsenko Cycle (M-Cycle), developed by Valeriy S Maisotsenko [14] is a thermodynamic system that uses the latent heat of vaporization of water to cool the product air stream. Due to its potential for dew-point evaporative cooling [1,15,16,17],

the cycle is well-known in the air-conditioning sector [18,19]. However, its use has lately been broadened in several energy recovery applications.

The M Cycle's working principle is to divert cooled air to the wet channel, which is then used as working air. It leads to a decrease in the working air's effective dry-bulb and wet-bulb temperatures in the wet channel. Warm outside primary air flows via the designated dry channels, transferring heat to the wet channels through the heat transfer surface. The temperature of the primary air at outlet will be below the wet-bulb temperature of the primary (ambient) air at input. The secondary air is the same as the outside air and travels via designated dry channels, but it also has several routes into the wet channels, where evaporated water is absorbed as moisture through mass convection. It may be assumed that the secondary air in each component of the equipment is continually increasing its moisture content until it reaches the exit. While it allows the product air temperature to approach the ambient air dew-point temperature in one mode, it also serves as a humidifying recuperator in another. It may therefore be utilized in HVAC and cooling applications as both cooler and humidifier heaters.

Coolerado Corporation has developed and commercialized several system designs based on the M-Cycle idea for diverse cooling and air conditioning applications [20,21].

The fundamental benefit of the M-IEC is that it cools primary air without changing the moisture content almost to sub wet-bulb temperatures. Some of the associated challenges are drawbacks include improvement of water and air distribution through the channels, optimizing space to simplify the overall system design, and also optimizing the construction costs while maintaining cooling efficiency [53].

### 1.3 HRV/ERV

Buildings and their HVAC systems must be energy efficient to meet the growing need for improved indoor air quality, performance, and environmental preservation. The purpose of HVAC design in buildings is to offer inhabitants good comfort and air quality across a wide range of outdoor conditions. For the health of the occupants, adequate fresh air supply via ventilation is required. Energy use by the HVAC sector amounts to 33% of overall energy consumption in most industrialized countries [55]. It is therefore critical to recover this energy by using a heat or energy recovery system in building applications.

Heat recovery refers to an air-to-air heat or energy recovery system, which is defined as the process of recovering energy (heat/mass) from a high-temperature stream to a low-temperature stream that is both effective and economic to operate [56]. A typical heat recovery system in a building consists of ducts for incoming fresh air and outgoing stale air, a heat exchanger core, which transfers heat or energy from one stream to the other, and two blower fans, one of which is used to exhaust stale air and the other to supply fresh air via the heat exchanger core. A typical heat recovery system placed in a ventilation system is shown in Figure 3. The expelled air pre-heats or pre-cools the fresh air stream in the core, which is then supplied to the interior parts of the buildings (depending on the season). In the heat exchanger, the outgoing and incoming air travel adjacent to one other but do not combine.

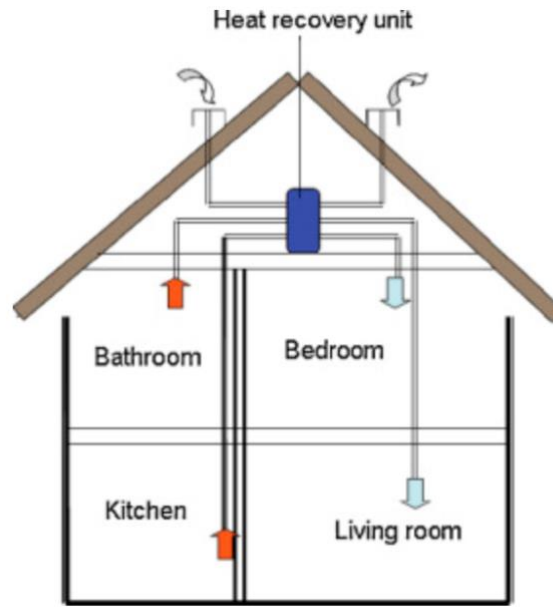


Figure 3: A heat recovery system [57]

Various types of heat recovery systems, such as fixed plate, heat pipe, rotary wheel, and run-around coil, have been employed to collect energy between supply and exhaust airflows throughout the previous few decades. Recently, Gendebien et. al. [58] used both numerical models and experimental methodologies, to address the issue of frost development in air-to-air heat recovery systems specialized in single room ventilation. The creation of a frost coating on the surface of such heat exchangers has been well known to cause an increase in thermal resistance and a reduction in flow section, resulting in a decrease in overall unit performance. By establishing the position of shifting borders, this study provided a three-zone model that included a dry, wet, and frost zone. Each zone was treated separately, and the proportional fraction of each zone was governed by the temperature of the exchanger wall. Experiments were conducted on a U-flow heat exchanger having 30° corrugations in the central part. Tests conducted under high relative humidity air supply conditions demonstrated an evolution that differs from that anticipated by the model. This was due to the condensates coming out of the heat

exchanger, which disrupted the predicted development of frost. When the wet section was smaller, the impact was minimized.

The energy recovery ventilator (ERV) is one of the green technologies classified by ASHRAE that works by recovering or extracting energy from one airstream (the regeneration airstream) and transferring it to another (the process airstream). Heat and moisture are transferred from the hot/humid side to the membrane surface via convection. Membrane heat exchangers are one of the most common types of fixed plate ERVs used in HVAC systems today. The membrane is a thin material that can be found in a variety of forms, including regular paper, tailored porous materials, and polymers [62]. The heat then conducts over the membrane, while moisture diffuses through the porous membrane. Finally, convection transfers the heat and moisture that are diffused and/or conducted through the membrane to the colder, less humid streamside. These processes produce cooler, less humid outside fresh air that is sent to the cooling coil without using any more energy. An ERV system's key advantages are that it is a static device with no moving components, is easy to build, and can be easily retrofitted [59].

In cold regions, the search for optimal mechanical ventilation of well-insulated residential structures must consider the minimal criteria for interior air quality, occupant thermal comfort, and heating energy savings [60] which necessitates the need for high energy efficient ventilation with heat/energy recovery systems. A significant amount of research has been underway in predicting and improving the effectiveness of fixed plate ERVs, as well as studying heat and moisture transport mechanisms across their membrane surfaces [61]. Nasif et al. conducted both experimental and computational research while developing mathematical models to estimate the performance of latent heat recovery heat exchangers in traditional air conditioning systems. They used laboratory-



scale permeability tests to assess membrane moisture transfer resistance [63]. They found that utilizing porous papers, which recover both latent and sensible heat, saved 78% more energy than using Mylar plastic film, which only recovered sensible heat in hot climates. The thermal performance of a counter-cross flow plate heat recovery exchanger was examined by Li et al. [64] using two alternative placement options (vertical and horizontal). They concluded that the vertical placement method outscored the horizontal mode in terms of thermal performance. In recent years, several research groups have been working towards addressing the concern of condensation and frosting in ERVs. While frost formation requires extremely low temperatures, condensation can occur even in mild winter weather conditions. Based on prior laboratory-controlled observations, Li et al. [65] presented novel correlation-based models of the thermal performance of single-core and dual-core ERV units during normal operation and defrost by recirculation operation. In comparison to the case without an ERV and the pre-heating defrost, the dual-core ERV lowered heating energy usage and provided a constant outside airflow rate in compliance with standards.

#### 1.4 Recent advances in indirect evaporative cooling

Numerous reviews of evaporative cooling are available in the literature [13,24-28]. However, most reviews concentrated on direct evaporative cooling and its prospective uses in thermal management in solar systems, building applications, and motor vehicle engines, among others. In recent years, there has been a greater emphasis on IEC development. Indirect evaporative cooling has been identified as one of the promising alternatives to traditional air conditioning, particularly in the desert and semi-arid environments [22,23]. Furthermore, it has begun to be used for fresh air pre-cooling under hot and humid climatic circumstances. When compared to vapor-compression air

conditioning systems, this technique is much more advantageous because it does not utilize compressors or high global warming potential refrigerants. Several studies on the indirect evaporative cooler (IEC) have been done over the last few decades to assess its viability, improve thermal performance, and expand its application regions.

Numerous numerical and experimental investigations on in-direct evaporative cooling technology have been undertaken during the last few years.

#### 1.4.1 Numerical Work

Rampazzo et al. [29] developed a First-Principle Data-Driven model for IEC. A Matlab-based simulation environment was constructed to depict the main aspects of the system, such as heat exchanges, and air and water temperatures, and to better comprehend changing system responses. They employed a static Moving Boundary (MB) technique that segmented the evaporative heat exchanger based on the physical events that occurred inside it. They established two models: the NOEVAP model, which defined the parts of the heat exchanger where the secondary channels were not wetted by the water film, and the EVAP model, which described the parts of the heat exchanger where the evaporative process occurred. The parameters of the model were calibrated using actual data. In addition, a simulation environment based on Matlab/Simulink was created. The advantages of using the simulation environment were twofold: they could generate synthetic data related to some fundamental aspects of IEC system thermal behavior, as well as understand parameter influence during the process; they could also design and test control strategies to efficiently manage the IEC system and evaluate its performance using simulations. Pandelidis et al. [30] proposed retrofitting a conventional recuperator as a counter-flow IEC. The IEC heat and mass exchanger was

followed by a traditional vapor-compression cooler, just like a standard recuperator, in the proposed system. The main difference was that the exhaust air channels were wetted with water. By simply adding a water distribution system, which includes nozzles, a tank, and a pump, the proposed approach could be employed in practically all existing recuperators. Using the  $\varepsilon$ -NTU-model, it's potential as a heat recovery mechanism in air conditioners was studied in a temperate climate. It was demonstrated that the redesigned system is far more energy-efficient than the ordinary recuperator. Furthermore, when compared to traditional recuperators, the proposed system could achieve a significantly larger temperature drop.

Hao et al. [31] developed a heat current model by introducing a new parameter known as the moisture-temperature ratio. This ratio combined humidity and temperature differences to depict heat and mass transport simultaneously. The moisture-temperature ratio allowed the driving potential of the linked heat and mass transfer processes to be assessed and changed as the difference between the hot fluid input temperature and the cool wet air inlet wet-bulb temperature. Wang et al. [32] performed a numerical analysis of two IECs and revealed that the crossflow regenerative HMX outperforms conventional cross-flow HMXs at low supply airflow rates for stand-alone HMXs. As shown below in Figure 4, the regeneration process involves removing a portion of the primary air from the outlet and using it as secondary air. Because the secondary air has already been cooled, the associated WB temperature is lower than the WB temperature of ambient secondary air, and the primary air-cooling limit has decreased considerably. For high supply airflow rates in multistage evaporators, the traditional HMX is preferable during the first stage as a pre-cooler, whereas the R- HMX is preferable during the second stage as a re-cooler.

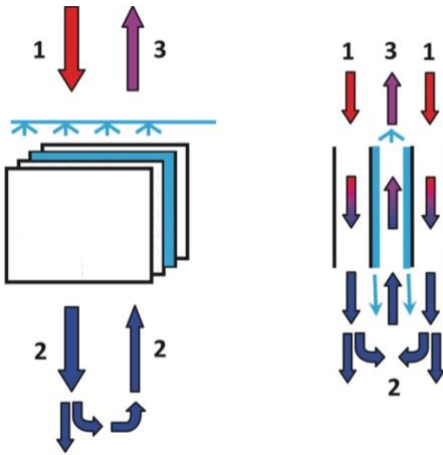


Figure 4: Working principle of a regenerative IEC equipment [13]

Guo et al. [33] devised a 2D mathematical model for a plate crossflow IEC considering the condensation area ratio. The problem was solved using Matlab and the finite difference approach for several states of condensation, such as total condensation, partial condensation, and no condensation.

Interesting work was done by Wan et al. [34]. They proposed a numeric model based on energy and mass balance to predict condensation from the primary air. The numerical model was confirmed with excellent agreement using computational and experimental data from the literature. In the dry channel, precise simulations were run to observe and examine the condensation instances, which included non, partial, and full condensation in the dry channel. Variable operating circumstances, such as primary and secondary air velocity, inlet temperature, humidity ratio, and wettability factor, were used to evaluate the IEC system's performance. The findings revealed that operating parameters such as humidity ratio, inlet temperature, velocity, and wettability factor influenced the three condensation states in the primary air channel.

## 1.4.2 Experimental Work

Numerous experiments have been conducted in the past years focused on improving performance for diverse climates by optimizing geometric parameters and flow configurations for various IEC systems. Additionally, substantial research has been conducted into the integration of IECs with other cycles. The effect of many performance characteristics such as condensation, as well as system configuration, has remained a research area of interest. Findings from experimental work on IECs have been discussed further below.

### *Effect of System Configuration*

Several attempts have been made to achieve high dew point and wet bulb effectiveness, and cooling capacity while considering the operating conditions and design configurations of the indirect evaporative cooling system. The effectiveness can be defined as follows:

$$\varepsilon_{wb} = \frac{T_{pin} - T_{pout}}{T_{pin} - T_{wb_{in}}} \quad (1)$$

$$\varepsilon_{dp} = \frac{T_{pin} - T_{pout}}{T_{pin} - T_{dp_{in}}} \quad (2)$$

Where  $T_{pin}$  and  $T_{pout}$  refer to primary side inlet and outlet temperatures respectively,

$T_{wb_{in}}$  and  $T_{dp_{in}}$  refer to the wet-bulb and dew-point temperatures at inlet respectively.

Cross and counter-flow evaporative coolers are the most common design configurations studied by research groups.

Bruno et al. [35] concluded that counterflow indirect evaporative cooler can supply air at temperatures equivalent to refrigeration systems with better thermal efficiency. It was

shown that the average wet-bulb effectiveness was about 106% for residential and 124% for commercial applications. The effectiveness exceeding 100% signifies that sub wet-bulb cooling conditions were achieved i.e.  $T_{pout}$  was lower than  $T_{wb_{in}}$ . Riangvilaikul and Kumar [17] developed a novel dew point evaporative cooling system for air conditioning applications and conducted experiments to investigate the outlet air conditions and system effectiveness at various inlet air conditions (temperature, humidity, and velocity) covering dry, temperate, and humid climates. The wet-bulb effectiveness ranged between 92 and 114 %, while the dew point effectiveness ranged between 58 and 84 %. Zhan and Changhong et al. [36] also performed a comparative study on dew point evaporative coolers with cross-flow and counter-flow IECs. According to their findings, the counter-flow configuration increases dew point efficiency by 15%, wet bulb efficiency by 22.5 percent, and cooling capacity by up to 20%. The COP of the cross-flow design, however, was 10% greater than that of the counter-flow layout. It can be deduced that a counter-flow design provides greater cooling effectiveness than a cross-flow one. However, the counterflow configuration improves system compactness.

#### *Effect of Operating Conditions*

Operating conditions are critical elements for improving performance and effectiveness. The primary and secondary air stream temperature, flow rates, humidity ratios, and plate wettability constitute the essential operating characteristics [37]. Zhan et al. [40] utilized numerical analysis to investigate the effect of these operating parameters on cooling effectiveness and cooling capacity. They suggested design conditions for the UK environment that have wet bulb and dew point effectiveness of up to 130 % and 90 %, respectively. Khalid et al. [38] and Zhan et al. [1] performed experiments for similar

inlet conditions where Khalid's group showed a better effectiveness value for an improved cross-flow dew point evaporative cooler. In general, it was observed that a higher inlet air temperature and lower inlet humidity ratio results in higher cooling effectiveness. Adam et al. [54] studied the effect of plate wettability on the cooling process and condensation. Within IEC, a numerical model based on energy and mass balance. When the wettability factor was reduced to 0.5, condensation was delayed, and the amount was reduced to 0.52 g/kg instead of 1.32 g/kg when the factor was 1. When the factor was dropped from 1 to 0.5, the average temperature at the output increased from 20.2 to 23.4 degrees Celsius.

The effect of feed water temperature on cooling effectiveness was found to be negligible [38-42]. The effectiveness increases with an increase in working to intake air ratio owing to the increased heat and water absorption capacity of working air. While cooling capacity increased with an increase in inlet air velocity, cooling effectiveness increased with a decrease in velocity, which resulted in a possible decrease in supply air temperature. This is because the contact duration between the air and the moist surface increases, increasing evaporation rate. In comparison to cooling capacity, the sensitivity of cooling effectiveness to changes in velocity was quite modest. Increased cooling capacity could be achieved at the expense of a negligible increase in supply air temperature. Additionally, a poorer coefficient of performance resulted when pressure drop increased with velocity. As a result, for increased cooler effectiveness and coefficient of performance, the inlet air velocity must be low.

### Effect of Geometry

There are three key geometric parameters to consider when designing a heat exchanger: channel height, length, and shape (square, rectangle, or triangle). In evaporative coolers, geometric characteristics have a significant impact on cooling performance. The geometry of both, the dry and wet channels affects the hydraulic diameter and the surface area, facilitating the heat transfer process. COP and primary outlet air temperature increase as the channel height rises, but the cooling effectiveness and cooling capacity decrease. However, having a small channel height implies more flow resistance, which lowers the energy efficiency.

Cui et al. [43] investigated the effect of some geometric parameters on the performance novel counter-flow closed-loop dew-point evaporative air conditioner by developing a computational model. The working channel is arranged in a closed-loop configuration. The working air enters the working dry passages first. It is then recirculated to the working wet channel and then expelled into the atmosphere at the end of the working dry channel. Working air can be pre-cooled before entering the working wet channels by using this setup. Because the air near the turning point (Figure 5) has a lower wet-bulb temperature than the incoming air, it has a significant cooling potential.

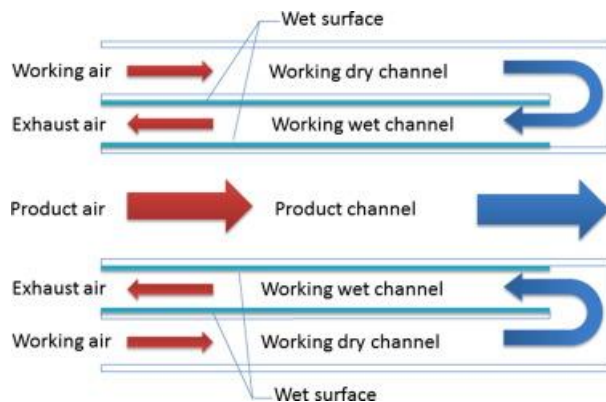


Figure 5: Schematic of the evaporative air cooler [43]



The product air is cooled by losing sensible heat to neighboring working wet channels, where the heat is absorbed by vaporizing the water and then supplied to the cooling space. To cool air below the wet-bulb temperature and close to the dew-point temperature, they suggested the following design conditions: inlet air velocity must be less than 1.5 m/s; length of the channel passage must be at least 200 times the height of the working channel; product channel height must be less than 10 mm; working channel height approximately half that of the product channel height, and product to working airflow ratio must be less than 1.5. Anisimov and Pandelidis [44] numerically compared rectangle, square, and triangular shapes of the channel. According to their study, if the channel heights were kept to a minimum, the triangle forms would be more successful than the rectangular ones. Later, Pandelidis et al. [45] investigated the effect of some geometrical parameters on the cooling performance of a regenerative HMX. They found that regenerative IECs benefit from a triangle-shaped channel. Flat channels, on the other hand, maybe a preferable option because triangle fins make it harder to disperse water evenly. Most of the works have been done by employing flat channels owing to its ease of construction. One interesting work done on triangular channels is by Kim et al [46]. By combining cellulose and PET to create a novel humidifying material, they devised a regenerative evaporative cooler (R-IEC) with triangular forms for dry and wet channels. While PETs gave stiffness to keep corrugation and form, cellulose disseminated the absorbed water in paper. Experimentally, they found that IEC units with triangular channels were more effective at removing moisture from the air and reducing pressure loss.

Literature suggests that for an optimal cooling performance and effectiveness, the dimensionless channel length should be at least 200 [1,36, 42, 43].

### *Effect of Material*

For indirect evaporative cooling systems, the characteristics of the evaporative material, such as its evaporation capacity, moisture absorption capacity, and diffusivity, have a higher impact on the cooling efficiency and performance of the system. An evaporative material layer is required in the IEC's wet channel to uniformly distribute and hold the water across the entire surface. As a result, the contact area between the working air and the wall will increase, allowing for greater sensible heat exchange between the dry and wet channels. An efficient material should have properties such as effective heat and mass transfer, low pressure drop, low cost, minimal bacterial development, and the ability to be formed in many geometries. Some of the commonly used materials are metals, ceramics, carbon, and zeolite. Zhao et al. [40] conducted a comparative analysis on all these evaporative materials and determined that the material's thermal properties had relatively little impact on heat and mass transfer efficiencies of exchangers. Shape formation/holding ability, durability, compatibility with water-proof coating, contamination risk, and cost are more relevant considerations.

### *Hybrid Systems and integration with other cycles*

Single-stage IEC's cooling performance is restricted by climate conditions; hence it was not widely employed at first. The IEC system has been integrated with other AC devices to accommodate higher cooling loads in buildings. Some of them are discussed below:

- i. Multistage IEC and DEC: A multi-stage evaporative system combines one or two IEC and direct evaporative cooler (DEC) and is commonly used in hot and arid climates. According to the findings of Fikri et al. [47], the two-stage design can improve saturation efficiency while increasing the RH of the exit air and water usage. The greatest temperature decline occurred during the first stage when evaporation occurs.
- ii. IEC with inverted Brayton cycle: The inverted Brayton cycle (IBC) may effectively recover waste heat even at low source temperatures. IBC is being studied as a viable method for recovering heat from exhaust gases. A turbine, a heat exchanger, and a compressor are the three basic components of the IBC system. First, the exhaust gas is expanded in the IBC turbine to a sub-atmospheric pressure. On the one hand, the turbine's power is partially used in the compressor's compression task, and on the other hand, if the turbine has mechanical energy left over, it can be exported via a shaft. The heat exchanger then cools the exhaust gas from the turbine, which helps to lower the compressor's energy consumption. Finally, the compressor raises the pressure of the exhaust gas to that of the environment. This, however, results in low thermal cycle efficiency. An inverted Brayton cycle is used with a counter-flow IEC to improve performance [48]. This system feeds the pre-conditioned working fluid into the compressor's inlet. The proposed system improved specific work production by up to 45% regardless of air inlet condition or turbine inlet temperature.
- iii. IEC with desiccant wheel: In order to attain comfort conditions in buildings with elevated latent loads, an effective and affordable hybrid system

consisting of a desiccant wheel integrated with IEC was presented as an alternative to conventional (direct expansion) systems [49]. The DW-IEC was shown to save 46.8 percent of energy throughout all climate zones, significantly more than the old system, and larger energy savings result in higher seasonal COPs for the new system.

- iv. IEC with Ground Heat Exchangers: The proposed system [50] was composed of three main parts: (1) the Ground Coupled Circuit (GCC), (2) the Cooling-Coil Unit (CCU), and (3) the IEC unit. The GCC, which was integrated with an IEC system, made up the hybrid cooling system. The fluid passed through the GCC and rejected its heat into the ground formation. When the circulating fluid left the GCC, it cooled down before entering the CCU. The ambient air, on the other hand, entered the CCU and transferred heat to the circulating cold water. Subsequently, it entered the IEC system, and, after the evaporation process, it cooled down and left the IEC system. Due to the supplemental cooling provided by GHE, the primary outlet air of IEC could meet cooling requirements and maintain a constant temperature in arid places like Tehran.
- v. IEC with humidification and dehumidification desalination cycle: In arid and hot climates, freshwater and cooling are two critical requirements. The purge air from IEC was provided to the humidification-dehumidification desalination (HDH) system to increase water productivity, taking full advantage of system integration. To attain the temperatures and humidity of the outlet air streams, a pilot IEC unit was first constructed and tested [51]. An IEC combined with a

humidification-dehumidification desalination cycle could reduce the supply air temperature below 25°C.

## OBJECTIVES

This study presents the numerical modeling of a cross-flow indirect evaporative cooling system for sensible cooling of air under different operating indoor and outdoor air conditions (temperature, humidity ratio and airflow rates) and the effects of other influential parameters (geometric parameters such as channel dimensions, airflow rates, the thermal conductivity of the separating plate). A simulation model has been developed for the heat and mass transfer. Experimental data validates the model's predictions for product air outlet conditions and system effectiveness. The validated model may hence be used to optimize and study system effectiveness under varied input air conditions.

# METHODOLOGY

## 3.1 Equipment Description

The tested heat and mass exchanger (HMX) was developed by Seeley International. The HMX is a modular heat exchanger constructed of polyethylene injected with biocide and capable of providing supply airflow rates of up to  $0.12 \text{ m}^3/\text{s}$  (260 CFM).

The system is comprised of an outdoor air intake and fan, an indoor air intake and fan, two air filters, an HMX section, condensate baffles, an exhaust air outlet, and a supply air input. Figure 6 depicts the flow paths of the return and supply air within the system. The system is divided into two distinct airflow routes. One enters the system as outside air through the fan, to be delivered to the cooling space, and the other, returns from the occupied space and exhausted as warmer exhaust air.

The HMX section consists of 5 cores, where one core is represented in Figure 6 and further explained in Figure 7. There are 42 pairs of channels in each core. Each pair of channel refers to a set of primary channel carrying product air on top and secondary air carrying working air on the bottom. Outside air is first routed via the HMX section's primary channels before being delivered to the cooling space. The air routed through this channel is hence also referred to as product air. Second, return air passes through the HMX section's secondary channels before leaving as exhaust air, also referred to as working air. The channels are symmetrically arranged about a central water trough that supplies water to the wet channels when the device needs to be operated for ERV mode. Each set of these channels on either side of the trough constitutes a section.

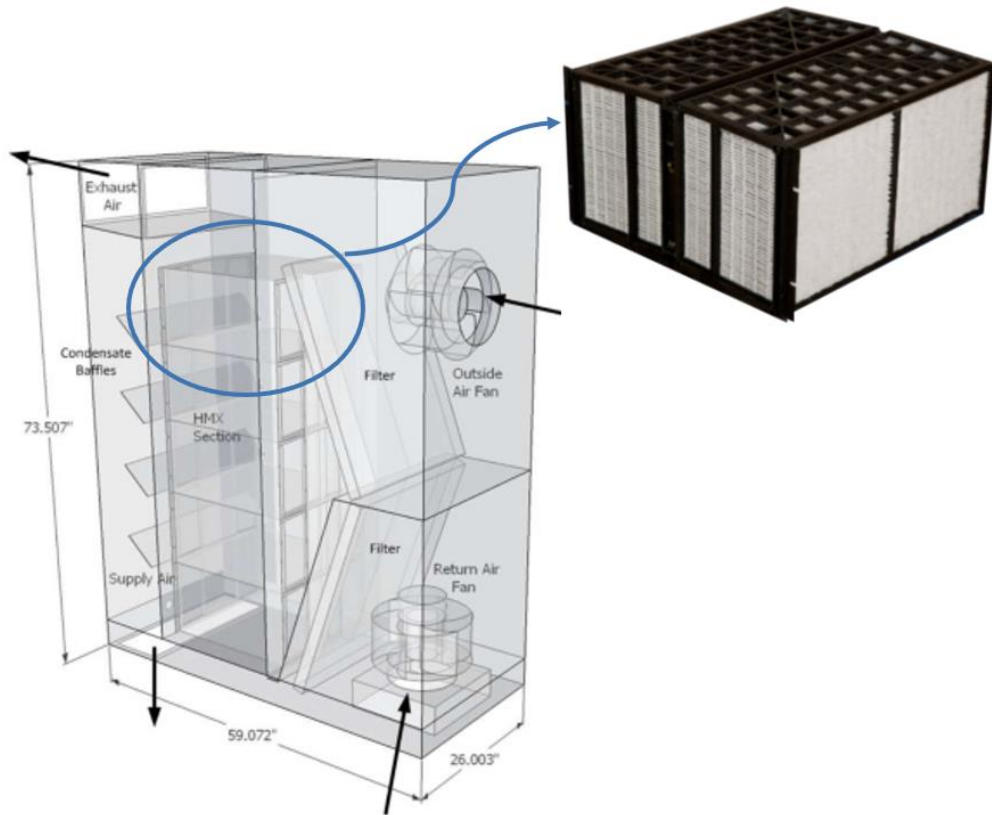


*Figure 6: Coolerado HRV/ERV schematic (sketch provided by Seeley) with zoomed-in view of single-core in the HMX section [66]*

The unit cell depiction of the HMX is shown in Figure 7. The unit cell is a portion of the HMX core that has been sliced vertically and then horizontally to isolate a single row. The shaded portion of both the parts depicted in Figure 7 correspond to the dry channel and represent one half of the core. Additionally, each airstream's three return, five supply, and twenty exhaust air channels are combined into a single channel. These channels have been illustrated as seen from the top, further below in Figure 10. The primary and secondary air exchange heat over two surfaces (1,2) in this depiction.



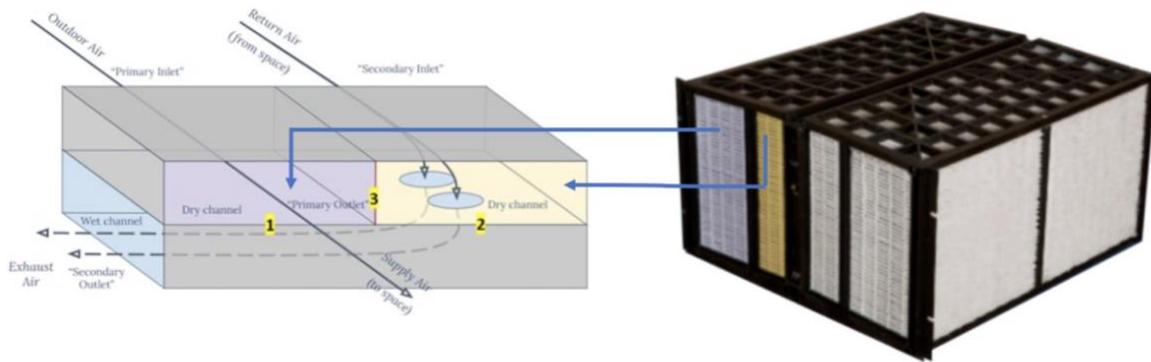


Figure 7: Unit cell representation of HMX (Sketch provided by Seeley)

Figure 8 illustrates the airflow pathways of the outdoor-to-supply (product) air and return-to-exhaust (working) air, as well as the wet and dry channels, in the HMX section. The return air (point 2 in the exploded view) flows parallel to the supply air (4 in the exploded view) before entering the wet channels via a series of successive holes along the channel's length. The return air is oriented in a crossflow direction relative to the supply air and travels via the wet channels. The supply air passes directly through the HMX and exchanges heat with the return air.

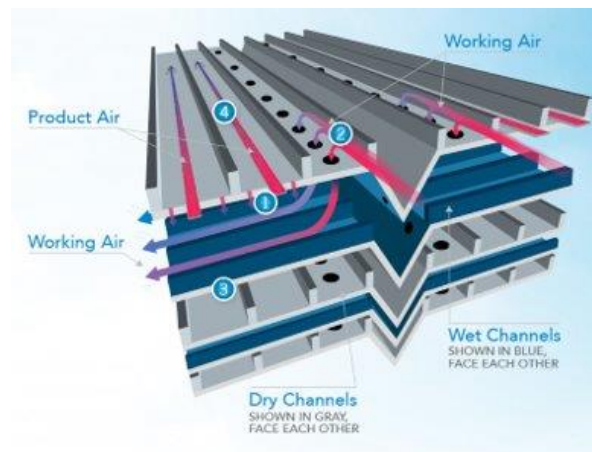


Figure 8: Exploded view of the HMX [66]

### 3.2 Test Matrix

**Acknowledgement of contributions** – The experimental design and plan was developed by WCEC R&D engineers Subhrajit Chakraborty and David Vernon. Subhrajit Chakraborty also lead and supervised the experimental campaign while being assisted by R&D engineer Robert McMurry.

Tests were performed for various outdoor and indoor conditions but only those with no occurrence of condensation were considered for the purpose of our analysis. Results from those have been used for the purpose of validation and hence details of instruments and their locations are not discussed here.

*Table 1: Experimental test points*

Primary/ Product/ Outdoor Air			Secondary/ Working/ Indoor Air		
Air Flow Rate(m <sup>3</sup> /s)	Inlet Temp. (°C)	Inlet Humidity ratio	Air Flow Rate(m <sup>3</sup> /s)	Inlet Temp. (°C)	Inlet Humidity ratio
0.556	27.46	0.0110	0.455	23.74	0.0078
0.593	27.41	0.0109	0.494	24.48	0.0120
0.610	35.39	0.0166	0.487	25.65	0.0123
0.420	26.48	0.0109	0.337	24.96	0.0079
0.410	26.98	0.0110	0.340	24.17	0.0095
0.410	27.01	0.0111	0.342	24.26	0.0102
0.356	34.85	0.0153	0.302	25.01	0.0108

Table 2: Test matrix for parametric analysis

Parameters	Baseline	
	Value	Range
Primary Air flow rate (m <sup>3</sup> /s)	0.5	[0.3,0.6]
Secondary Air flow rate (m <sup>3</sup> /s)	0.5	[0.3,0.6]
Primary Height (m)	0.003	[0.001,0.01]
Primary Length (m)	0.508	[0.05,0.5]
Secondary Height (m)	0.002	[0.002,0.01]
Primary Channels/ (Secondary Length)	20	[2,20]
Plate Conductivity (W/m-K)	0.25	[0.1,100]
Delta Plate (m)	0.0004	[0.00025, 0.00127]

Subsequent details on the validation and parametric analysis have been further discussed in section 4.

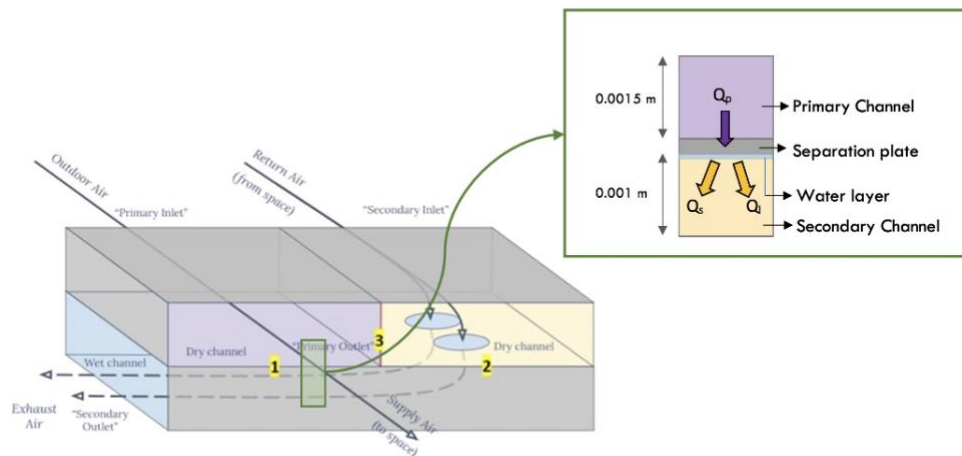
### 3.3 Governing Equations

A unit cell was selected for performing the heat and mass transfer analysis considering half heights each of the primary and secondary side about the separation plate wall. Suitable boundary conditions were chosen to set up the temperature and humidity distributions across the channels and energy balance was performed on each of these elements. The following assumptions were made:

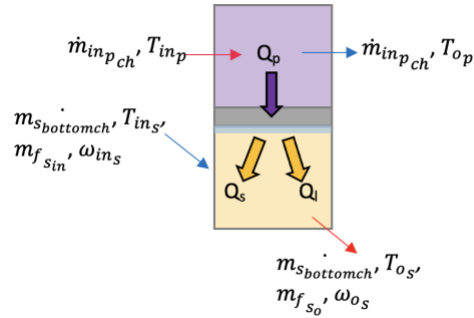
- Heat and mass exchange process for the model is at steady state,
- Air is regarded as an incompressible fluid,
- There is no heat transferred to the surroundings, the system is adiabatic,

- There is no temperature gradient across the plate separating the dry and wet channels and thus the elemental wall temperature is uniform. Literature reviewed showed that due to the plate wall's thin thickness, the thermal conductivity has minimal effect on the magnitude of the heat and mass transfer rates.
- The channel separators within the primary and secondary section are modelled as fins

For the segmental modeling, the domain considered was one set of rows of primary and secondary side and modeled as a cross-flow heat exchanger as shown in Figure 9. This includes 5 channels of the product/primary air, 3 channels of the working/ secondary air on the top and 20 channels of secondary air on the bottom.



(a)



(b)

Figure 9: Segment for dry-wet numerical analysis (a) Control volume as a part of the unit cell inset (b) Flow parameters entering and leaving control volume

Air in the secondary channels on the top passes through the holes and is distributed to the 20 channels on the bottom. This domain is divided into segments of 6 by 20 as depicted in Figure 10. By incorporating mass and energy conservation concepts for the control volume in Figure 9 (b) and domain shown in Figure 10, the heat and mass transfer within an IEC may be calculated as per equations mentioned in Section 3.3.2 .

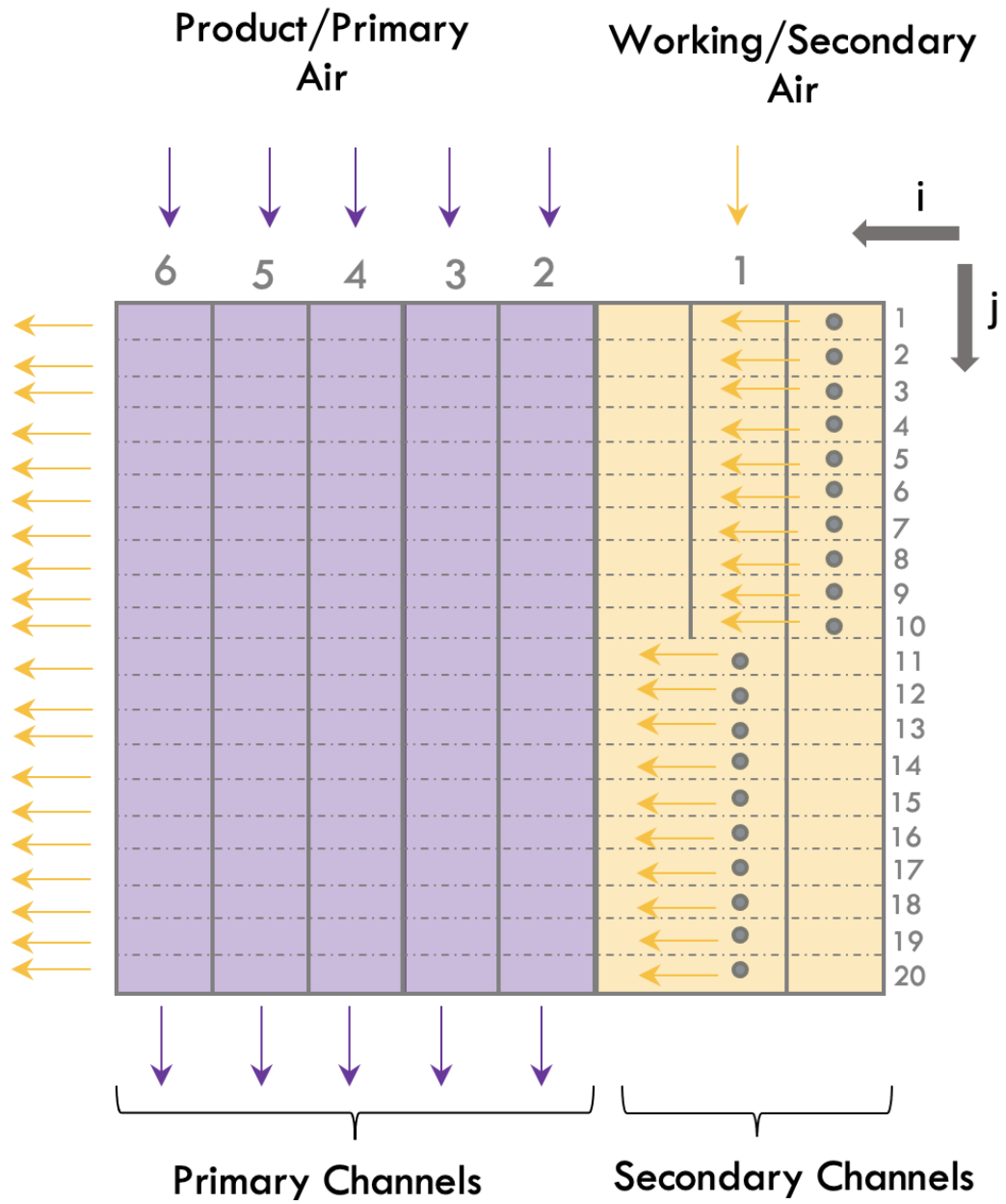


Figure 10: Air flow distribution in the channels for one half core (top view)

### 3.3.1 Model Inputs

Table 3: Geometric parameters of the IEC

Parameter	Value/Unit
$N_{core}$	5
$N_{rows}$	42
$N_{sections}$	2
$N_{chp_{halfrow}}$	5
$N_{chstop_{halfrow}}$	3
$N_{chsbottom_{halfrow}}$	20
$M$	6
$N$	20
$H_p$	0.003 (m)
$H_s$	0.002 (m)
$W_p$	0.022 (m)
$W_s$	0.022 (m)
$L$	0.508 (m)
$d_0$	0.005 (m)
$\delta_{fiber}$	0.0004 (m)
$\delta_{plate}$	0.0004 (m)
$h_{fp}$	0.0015 (m)
$h_{fs}$	0.001 (m)
$w_f$	0.003 (m)
$l_{fp}$	0.5 (m)
$l_{fs}$	0.13 (m)
$f$	0.5
$RelRough_p$	0.005
$RelRough_s$	0.01

Table 4: Flow inputs to the model

Parameter	Value/Unit
$k_{fiber}$	0.17 (W/m-K)
$k_{plate}$	0.25 (W/m-K)

$\dot{V}_{p_{total}}$	0.47 (m <sup>3</sup> /s)
$\dot{V}_{s_{total}}$	0.47 (m <sup>3</sup> /s)
$T_{in_p}$	308.2 (K)
$T_{in_s}$	297 (K)
$\omega_{in_p}$	0.017
$\omega_{in_s}$	0.009

$\omega$  refers to the humidity ratio defined as mass of water vapor per unit mass of dry air.

### 3.3.2 Equations

To perform the heat transfer calculation, an energy and mass balance approach was used to calculate the outlet temperatures and humidity ratio. Energy balances were performed for both the primary and secondary channels while mass balance for performed only for the secondary (wet) channel since there are no humidity changes in the primary (dry) channel. The same set of equations were used to model the entrance section of the secondary channel- the top channel. The major change was in the surface area since this channel had holes on its separation plate for air to be redirected to channels at the bottom. Due to arrangement of the holes, the area was divided into two halves with ten holes in each of these.

The mass balance equation is given by

$$\frac{\dot{m}_{s_{bottomch}}}{2} (m_{f_{sout}} - m_{f_{sin}}) = g_{m_{water}} * (m_{f_{wall}} - m_{f_{avg}}) * A_{unfinned_s} \quad (3)$$



*out* and *in* represent the exit and entrance of each sub-section used for calculation. *avg* denotes the average of the indicated parameter at the exit and entrance such that

$$m_{f_{avg}} = \frac{(m_{f_{sout}} + m_{f_{sin}})}{2} \quad (4)$$

$m_{f_s}$  represents the secondary channel air stream given by

$$m_{f_s} = \frac{\omega_s}{\omega_s + 1} \quad (5)$$

The mass fraction at wall is given as

$$m_{f_{wall}} = \frac{x_{f_{wall}} * M}{x_{f_{wall}} M_{water} + (1 - x_{f_{wall}}) M_{air}} \quad (6)$$

where  $x_{f_{wall}}$  is the mole fraction calculated using Dalton's law of partial pressures computed as

$$x_{f_{wall}} = \frac{P_{sat}}{P_{atm}} \quad (1)$$

$P_{sat}$  is the saturation pressure while  $P_{atm}$  is the atmospheric pressure at the wall temperature.

$M$  and  $M_{air}$  are the molar masses of air and water respectively.

The mass transfer conductance was calculated using the following equation

$$g_{m_{water}} = \frac{\rho_s * v_s * Sh}{Sc * 2H_s} \quad (8)$$

where  $Sh$  and  $Sc$  are the Sherwood and Schmidt number respectively. The Sherwood number was assumed to be equal to the Nusselt number, calculated using EES's inbuilt function while Schmidt number was calculated using the following equation

$$Sc = \frac{v_s}{d_{water-air}} \quad (9)$$

where  $d_{water-air}$  is the diffusion coefficient of water in air.

The participating area will not involve the channel separators modeled as fins, and hence the un-finned area has been used for the purpose of this calculation.

The general energy balance can be defined as follows

$$Q_p = Q_l + Q_s \quad (10)$$

$Q_p$ ,  $Q_l$  and  $Q_s$  denote the primary side, latent and secondary side heat transferred respectively.

The energy balance in the primary air stream can be defined using the equation below

$$Q_p = \frac{1}{R_{total}} * (T_{p_{avg}} - T_{wall}) \quad (11)$$

and further

$$Q_p = \frac{\dot{m}_{in_{p_{ch}}}}{2} * (h_{p_{in}} - h_{p_{out}}) \quad (12)$$

$R_{total}$  is the total thermal resistance entailing the conductive resistance offered to heat transfer by the plate, water layer and wicking fibers along with convective resistance due to the air in the channels. The *in* and *out* represents the entry and exit of the computational domain/ the subsection. The conductivities were obtained using the thermophysical property routine inbuilt in EES.

On similar lines, the energy balance in the secondary channel be outlined as follows

$$Q_s = \frac{htc_s}{2} * (T_{wall} - T_{s_{avg}}) * A_{total_s} \quad (13)$$

$htc_s$  is the heat transfer coefficient calculated from EES's inbuilt function.  $A_{total_s}$  is the total heat transfer area on the secondary side taking into account the fin efficiency and can be expressed as

$$A_{total_s} = (A_{finned_s} * \eta_{f_s}) + A_{unfinned_s} \quad (14)$$

The latent heat can be calculated by multiplying the total amount of water evaporated into the secondary air stream by the vaporization enthalpy, as shown in the equation below.

$$Q_l = g_{m_w} * (m_{f_{wall}} - m_{f_{avg}}) * \Delta h_{vap} * A_{unfinned_s} \quad (15)$$

The change in enthalpy of the secondary air stream will be equal to the total heat transferred from the primary side i.e.

$$Q_p = \frac{\dot{m}_{s_{bottomch}}}{2} * (h_{s_{out}} - h_{s_{in}}) \quad (16)$$

Equations (13), (15) and (16) can then be plugged back into equation (10) to complete the energy balance.

By solving these equations, the outlet temperatures and humidity ratios were obtained at the end of each subsection. These were then averaged out for the effectiveness calculations, namely dewpoint and wet-bulb effectiveness.

# RESULTS AND DISCUSSION

## 4.1 Model Validation with Experimental data

The outlet air conditions have a considerable impact on the comfort of a cooling space. The performance of an evaporative cooling system, i.e., wet bulb and dew point effectiveness, is primarily determined by the exit air temperature (product air) and the incoming air condition, as represented by equations (1) and (2). The higher the wet bulb and dew point effectiveness, the closer the outlet air temperature approaches the intake air's wet bulb and dew point temperature.

The humidity ratio of the product outlet air was not altered. Figures 11, 12, 13 depict a comparison of numerical and experimental data for the primary and secondary outlet air temperatures as well as the secondary air outlet humidity ratios.

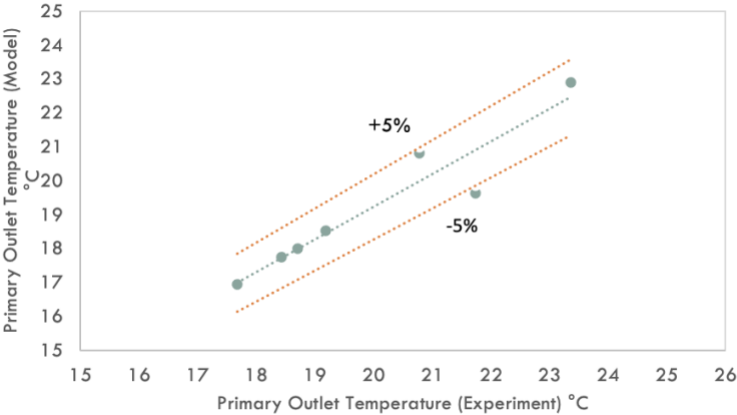
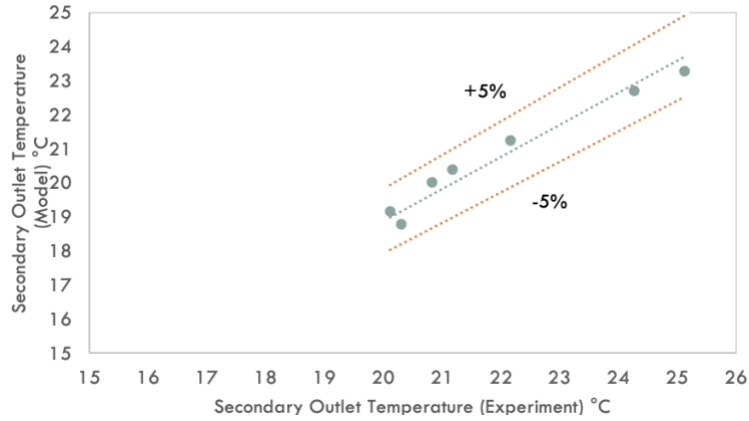
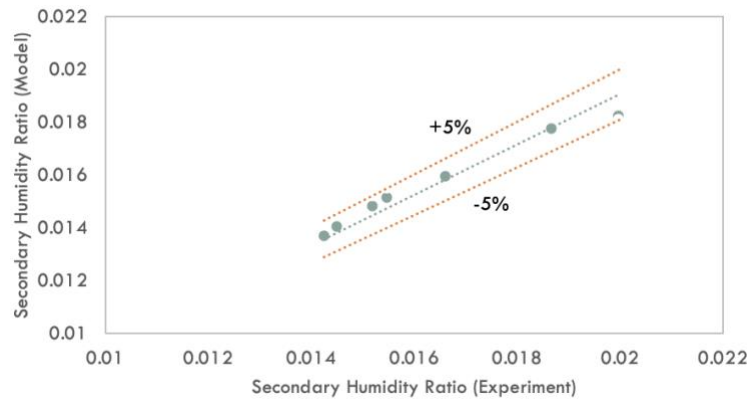


Figure 11: Comparison of model results with experimental data for Primary Outlet Temperature



*Figure 12: Comparison of model results with experimental data for Secondary Outlet Temperature*



*Figure 13: Comparison of model results with experimental data for Secondary Humidity Ratio*

The numerical model results align well with the experimental data. Comparisons were made only for cases where there was no condensation. The data plots show that the model can estimate the outlet air temperature to within 5% of the actual value. The calculated mean average errors MAE was 0.78°C in case of primary outlet temperature, 1.22°C in case of secondary outlet temperature and 0.0007 in case of the secondary outlet humidity ratios, confirming that the model fit the experimental data reasonably well. In practice, the

velocity, temperature, etc. are not uniform across the channel gap as specified in the modeling assumptions. The recorded temperatures at the channel's inlet and exit are average values applied to validate the model. According to the findings of earlier research [17,52], the error between projected values and experimental data ranges from 2 to 10%, which is similar to the findings of this study for outlet air temperatures and humidity ratios. To have a better understanding of the data and to determine whether the temperature averaging influenced the accuracy, a validation of core 5 was also performed. The simulated results were compared to temperature readings obtained from RTDs (Resistance Temperature Detector) installed at the primary and secondary exits of core no. 5. Three RTDs were used on the primary side - R1, R2, and R3, across five channels, while four RTDs were used on the secondary side - R1 through R4, across twenty channels. As a result, the primary side validation was significantly more accurate than the secondary side validation, owing to the model's secondary channel temperatures being averaged and compared to experimental values. Results are presented in Figures 14 and 15. Maximum deviation in model predictions of secondary side outlet temperature and humidity ratio was noted for higher CFM values of primary and secondary side. For both- the temperature and humidity ratio, the model slightly underpredicted the values. A possible reason could be that the sensors to number of channel ratio was higher for primary side as compared to secondary, hence the disparity. However, for the case of lower CFM on both sides, the deviation was found to be largest in the primary outlet temperature.

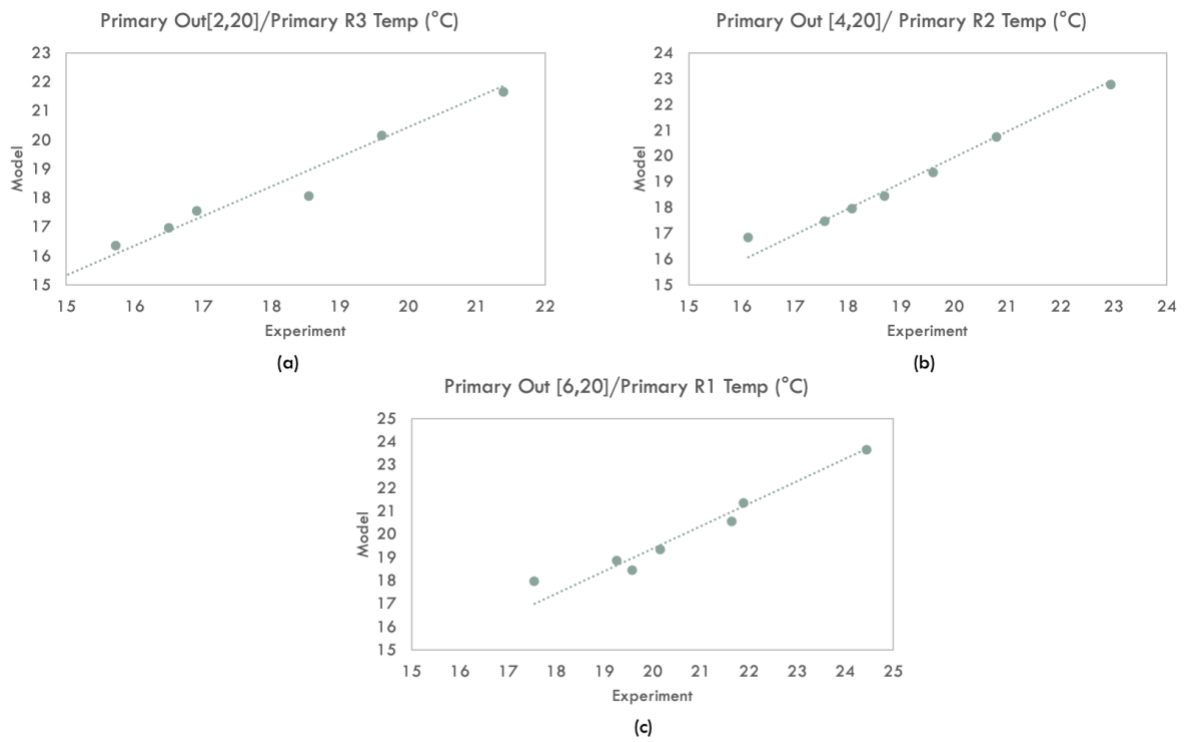


Figure 14: Model vs experimental data validation for core 5 for primary side.

The indices in the caption of each plot represents the position where model results were evaluated as per numbering scheme shown in Fig 5.

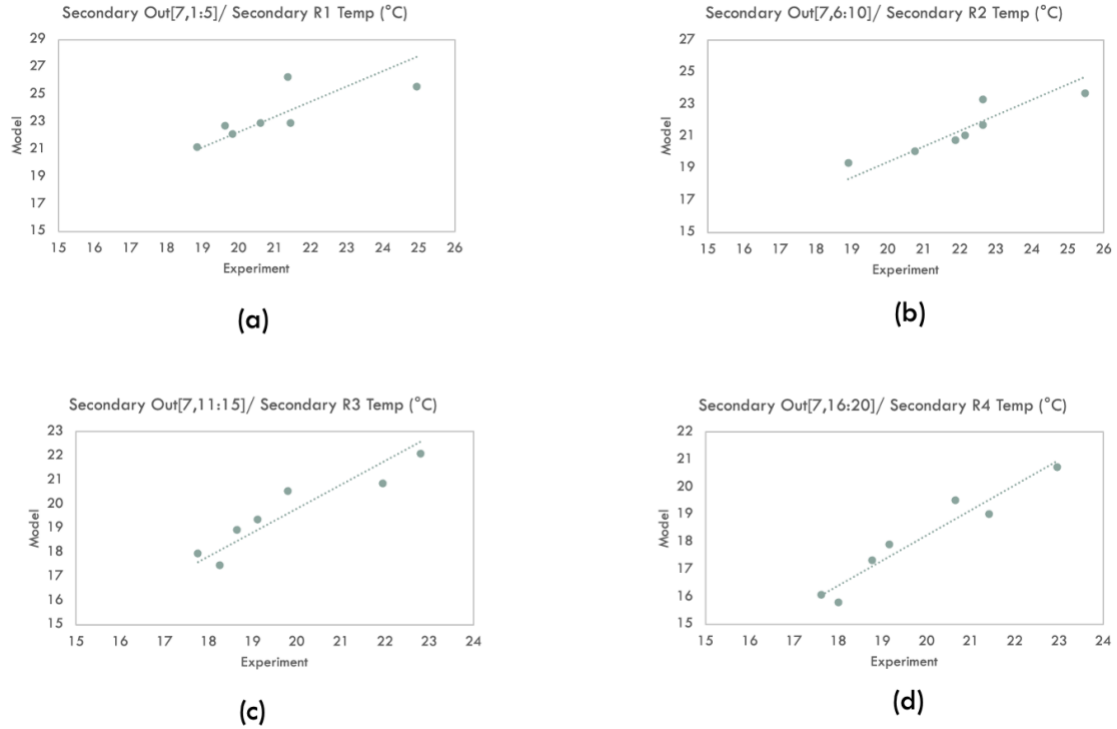


Figure 15: Model vs experimental data validation for core 5 for secondary side.

The indices in the caption of each plot represents the position where model results were evaluated as per numbering scheme shown in Fig 5. The range indicated by the second index represent the range of sectional channels across which the outlet temperatures were averaged.

## 4.2 Parametric Study

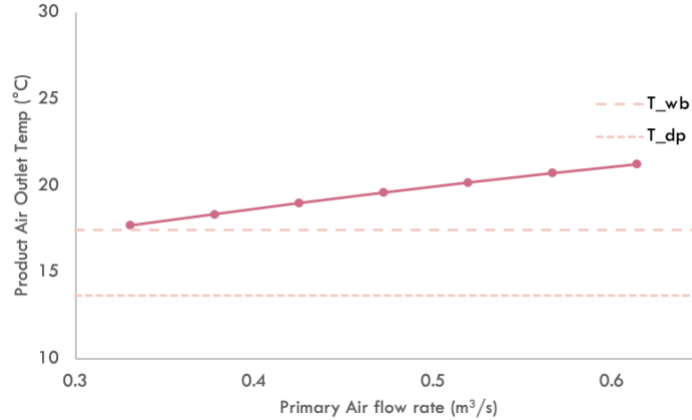
Understanding the effect of various parameters on cooling performance is critical for improving the heat transfer characteristics of IECs. The following section investigates the impact of some of the factors using the validated model. The parameter under study has been varied while keeping the rest at their baseline values as listed in Table 2. The performance metrics of the study are the product air outlet temperature, heat transferred, dew-point effectiveness, and wet-bulb effectiveness. The heat transferred in one channel of primary side is given by



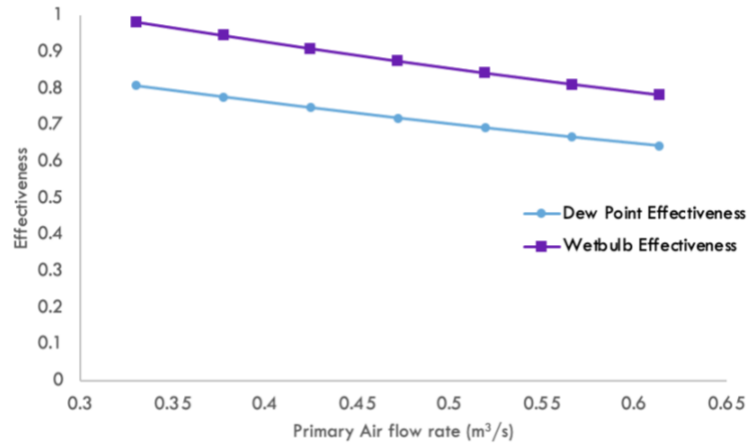
$$Q_p = \dot{m}_{in_p ch} * c_{p in_p} * (T_{in_p} - T_{op avg}) \quad (17)$$

#### 4.2.1 Primary air flow rate

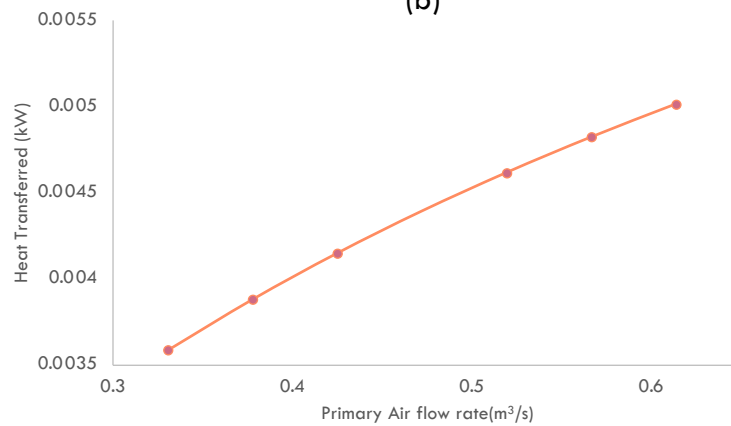
For this study, the volumetric flow rate of the primary/outdoor side was varied from 0.3 to 0.65 m<sup>3</sup>/s for a baseline value of 0.5 m<sup>3</sup>/s on the secondary side. An increase in the product (primary) air flow rate resulted in decrease in the dew-point and wet-bulb effectiveness of the system (Figure 16). This can be attributed to the decrease in the residence time in primary passage for heat to be exchanged with the wet channels. However, the heat transferred increased due to increased primary side mass flow rate of air overcoming the effect of higher outlet temperatures.



(a)



(b)



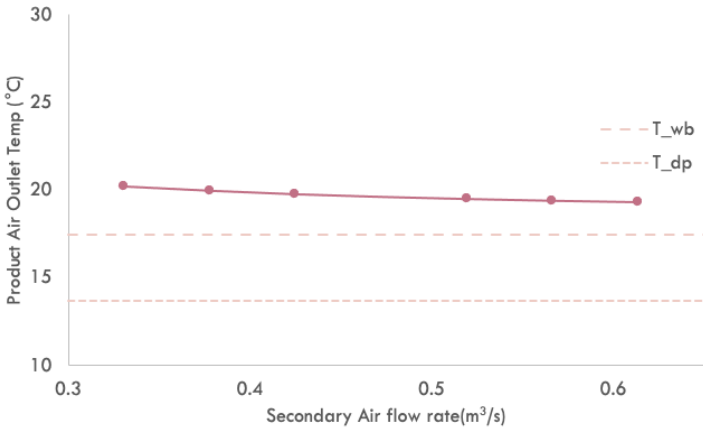
(c)

Figure 16: Effect of Primary airflow rate

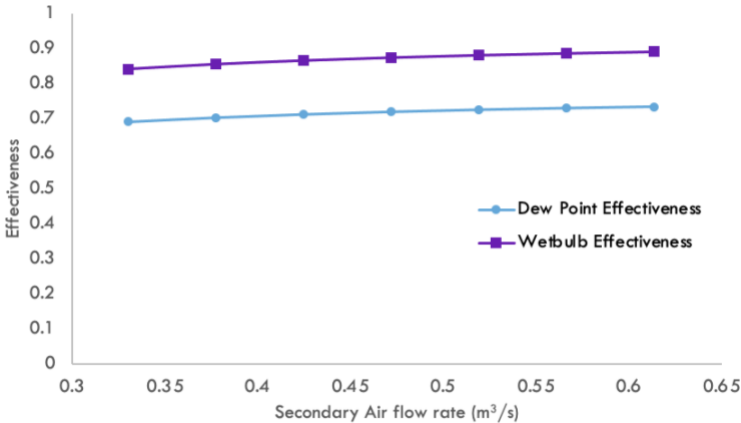
#### 4.2.2 Secondary air flow rate

Similar to the previous case, the volumetric flow rate of the secondary/outdoor side was varied from 0.3 to 0.65 m<sup>3</sup>/s for a baseline value of 0.5 m<sup>3</sup>/s on the primary side. In contrast, it was found that for the secondary side (Figure 17), the effectiveness was directly proportional to the air flow rate. This can be explained by increasing the air mass flow rate, which improves evaporative

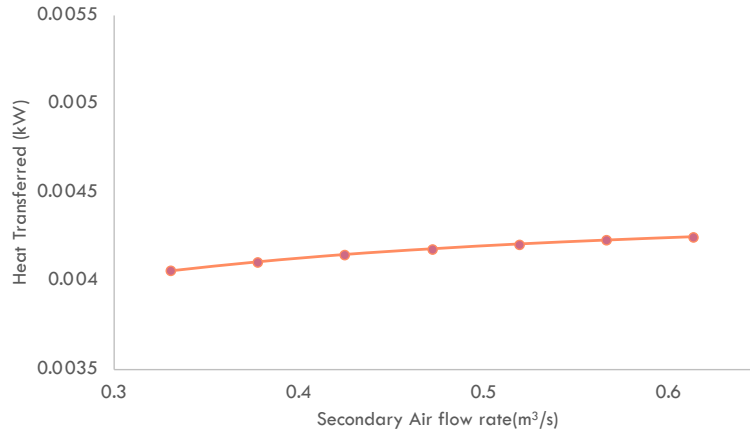
cooling on the secondary side, resulting in a reduction in the product air outlet temperature.



(a)



(b)



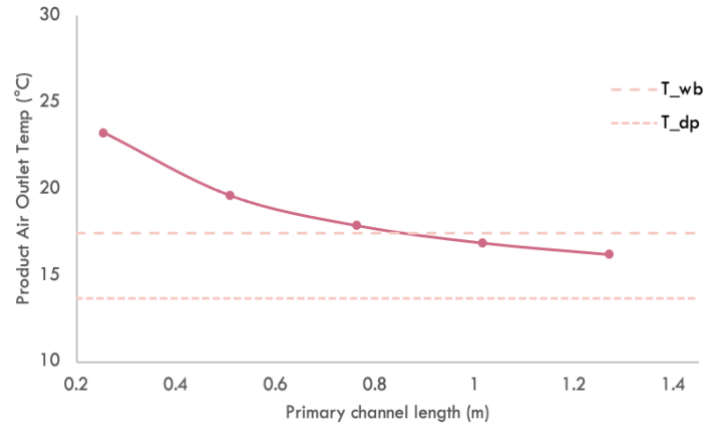
(c)

*Figure 17: Effect of Secondary air flow rate*

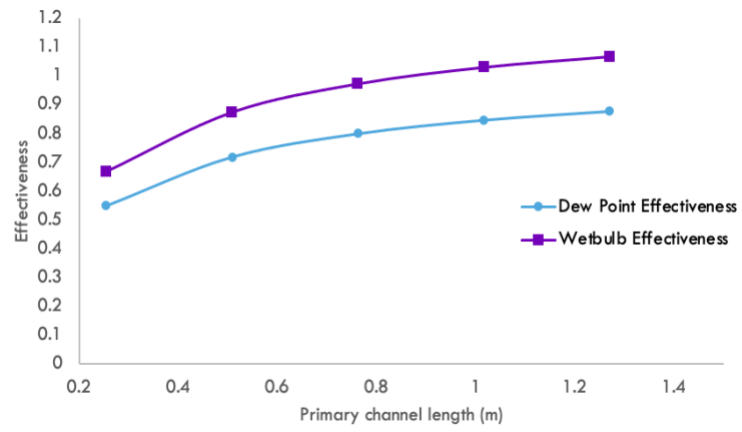
An increase in the heat transferred was also noted as a result of lower product air temperature at a fixed primary side air flow rate (Figure 17(c)).

#### 4.2.3 Primary channel length

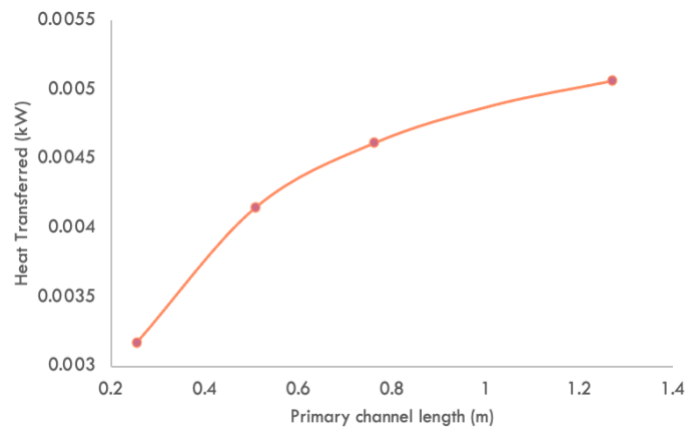
The primary side channel length was varied from 0.25m to 1.27m, maintaining a constant value of secondary channel length. It was seen that the dewpoint and wet-bulb effectiveness both increased owing to a longer residence time. Sub wet-bulb temperatures were achieved beyond 0.9m and consequently, wet-bulb effectiveness exceeded 1 (Figure 18(b)). There was a significant increase in heat transfer beyond 0.5 m (Figure 18(c)). However, the pressure drop also increases linearly and hence, the channel length needs to be limited based on the pressure drop constraints (Figure 18 (d)).



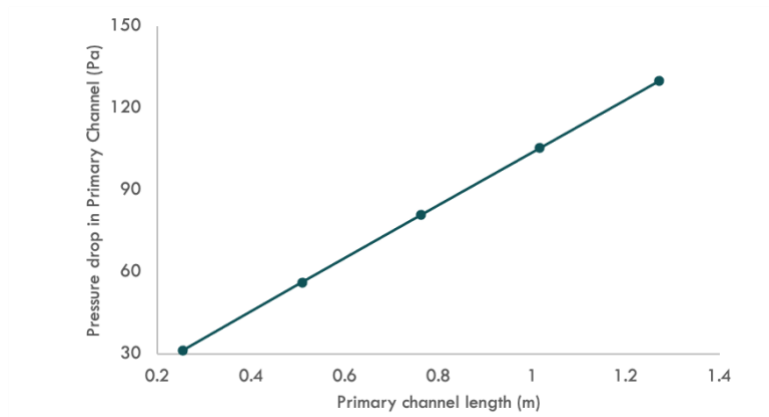
(a)



(b)



(c)



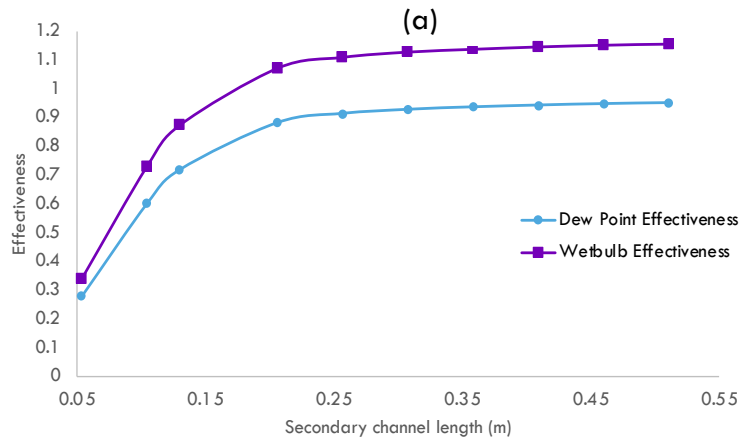
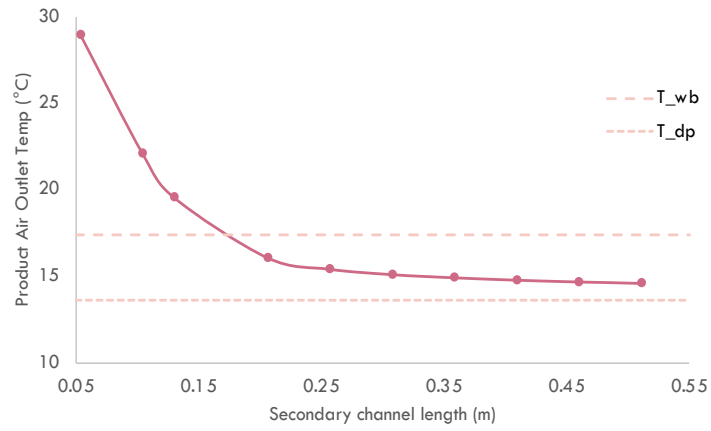
(d)

Figure 18: Effect of Primary channel length

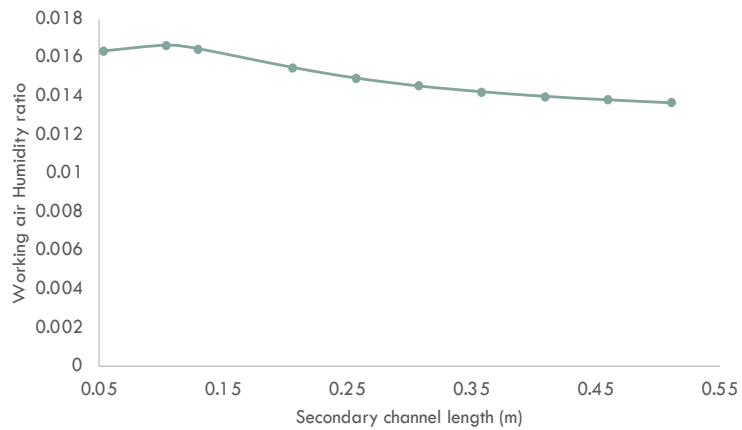
#### 4.2.4 Secondary channel length

The model defines the length of secondary channels as a function of the number of primary channel passages. The number of primary channels were varied from 2 to 20 corresponding to a secondary channel length of 0.05m to 0.5m. Although a similar increase in effectiveness trend was seen (Figure 19), there was one noteworthy observation. The initial growth was steeper than the subsequent readings, which gradually achieved a constant value. This can be explained by examining the product air temperature plot, which hits a minimum value after which there is a steady descent. This is because as the channel length rises, the working air in the secondary channel approaches saturation, and evaporative cooling may no longer be efficient, resulting in a stagnant product air temperature. This is also supported by decreasing working air humidity ratio values (Figure 19 (c)), as opposed to the values obtained by increasing primary

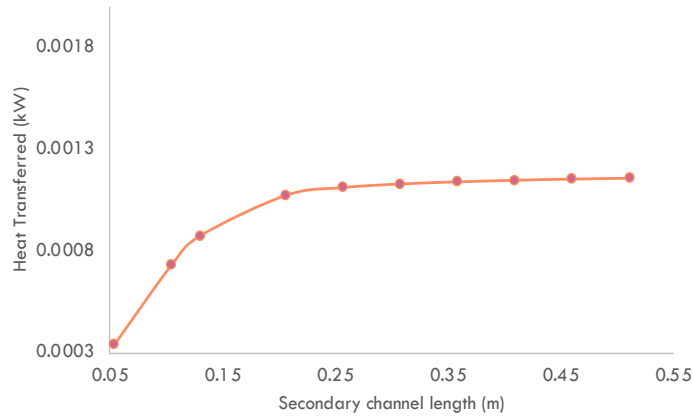
side channel length. Similar to the other trends, the heat transferred increased initially and became steady beyond 0.25 m .



(b)



(c)



(d)

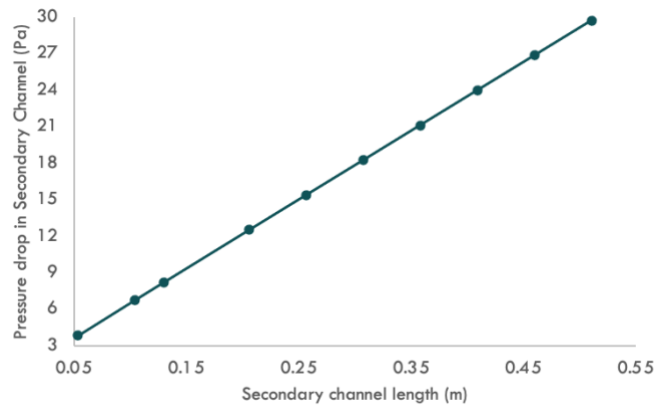
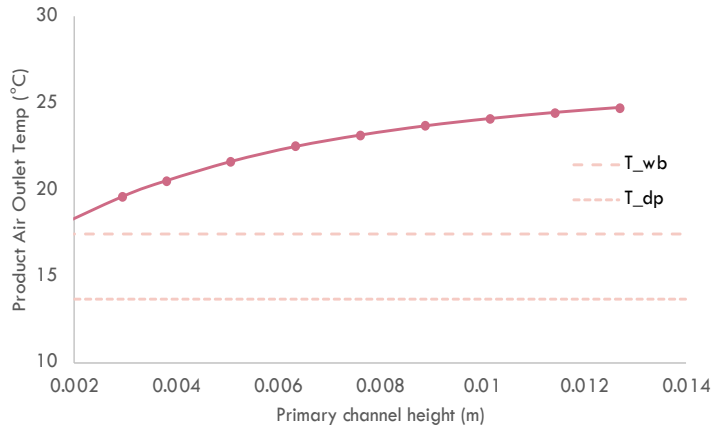


Figure 19: Effect of secondary channel length

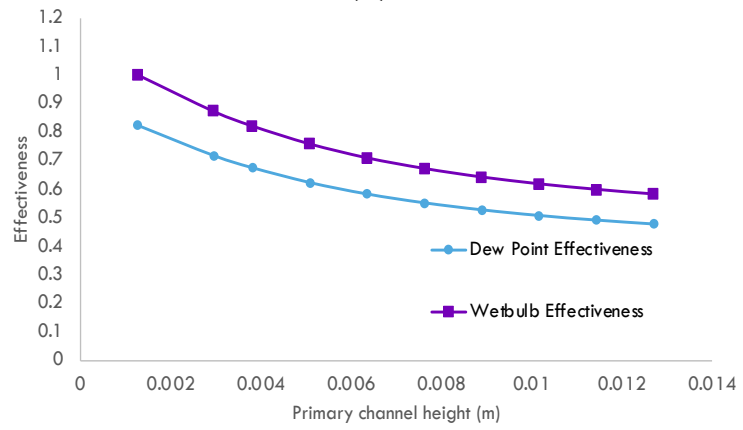
#### 4.2.5 Primary channel height

It was found that increase in primary channel height from 0.001 to 0.014m corresponding to secondary channel height of 0.002m resulted in a decrease in the dewpoint and wet-bulb effectiveness values as seen in Figures 20. Increasing the height resulted in a smaller pressure drop, consequently lower velocity and hence lesser heat transfer.

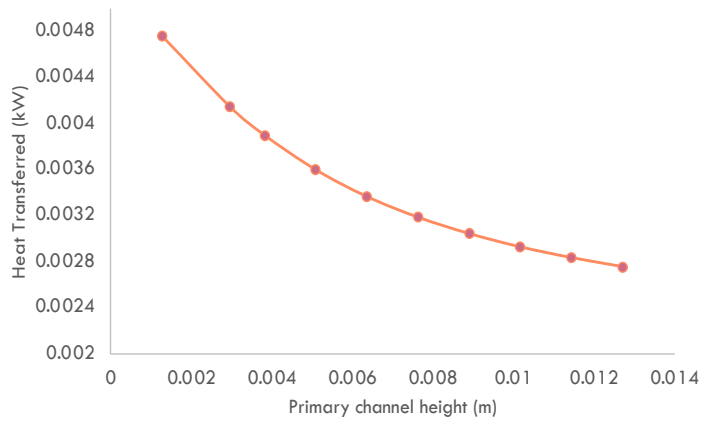




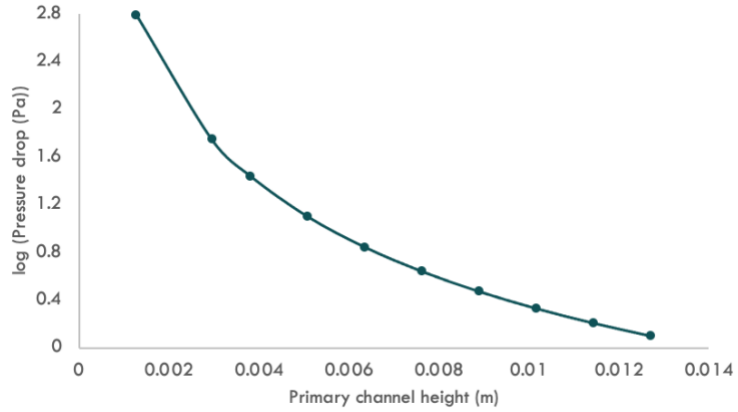
(a)



(b)



(c)

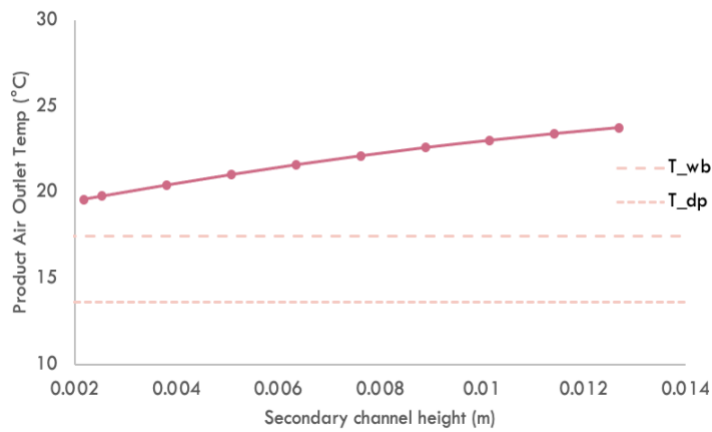


(d)

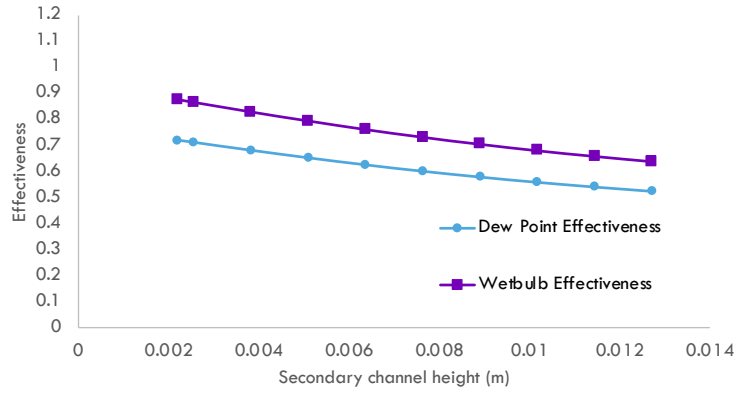
Figure 20: Effect of Primary channel height

#### 4.2.6 Secondary channel height

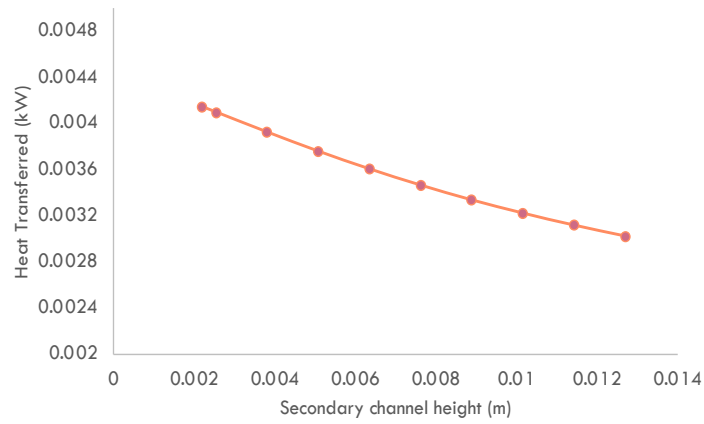
It was found that increase in secondary channel height from 0.002 to 0.01m corresponding to primary channel height of 0.003m resulted in a decrease in the dewpoint and wet-bulb effectiveness values in addition to the heat transferred as seen in Figures 21. The explanation in the previous section holds true for the effect of secondary channel height.



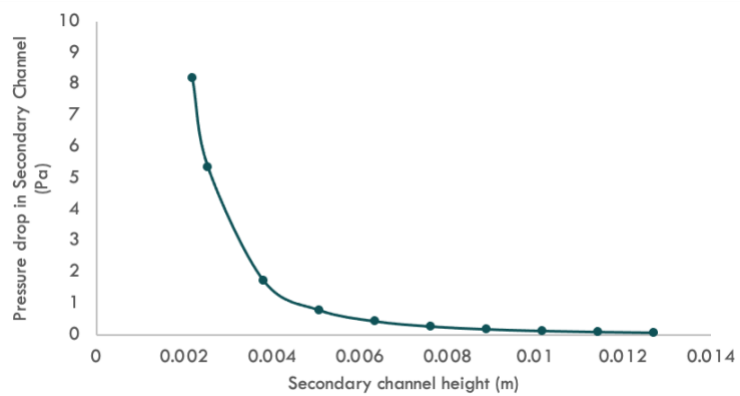
(a)



(b)



(c)



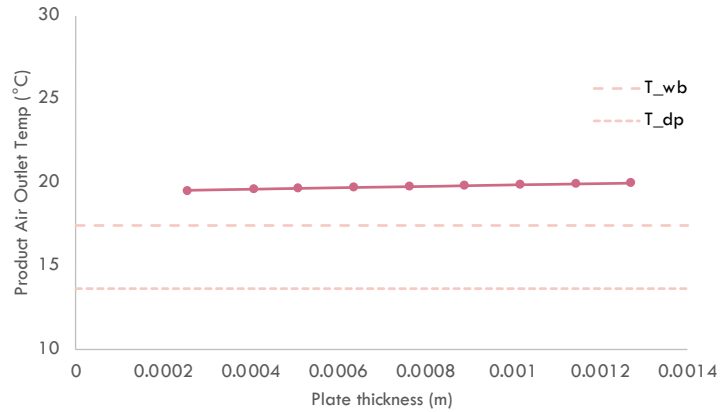
(d)

Figure 21: Effect of Secondary channel height

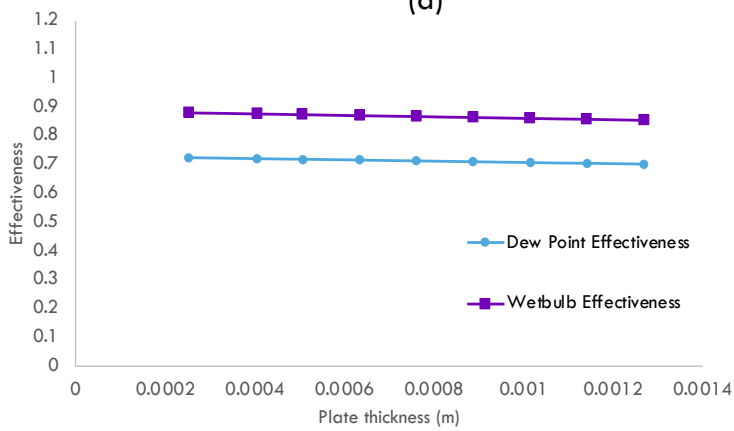
Smaller channel height, however, would result in higher flow resistance, which would necessitate more pumping power and, eventually, a loss of energy efficiency. This can be confirmed by the pressure drop which drastically increases approximately below 0.004 m (Figures 20(d) and 21(d)). Hence, there needs to be a trade-off between these two constraints.

#### 4.2.7 Plate thickness

As the separation plate thickness is increased from 0.00025m to 0.00127m, the conduction resistance increases resulting in higher product air temperature and consequently lower effectiveness. Although, the effect of varying plate thickness is not very pronounced as seen from the simulation results in Figure 22.



(a)



(b)

Figure 22 :Effect of plate thickness

#### 4.2.8 Plate conductivity

As discussed in section 1.4.2, it was validated that the thermal conductivity of the material had a negligible effect on the system performance (Figure 23). The conductivity was varied from 0.1 W/m-K with smaller intervals up to 5 W/m-K followed by larger intervals up to 100 W/m-K. The baseline value considered for rest of the study was set to 0.25W/m-K. An evaporative material layer that can evenly distribute and hold water across the entire region is required in the IEC's wet channel. This increases the contact area between the working air and

the wall, allowing for a more perceptible heat exchange between the dry and wet channels. An efficient material should have properties such as good heat and mass transmission, low pressure-drop, low cost, resistance to bacteria development, and the ability to be formed in myriad geometries.

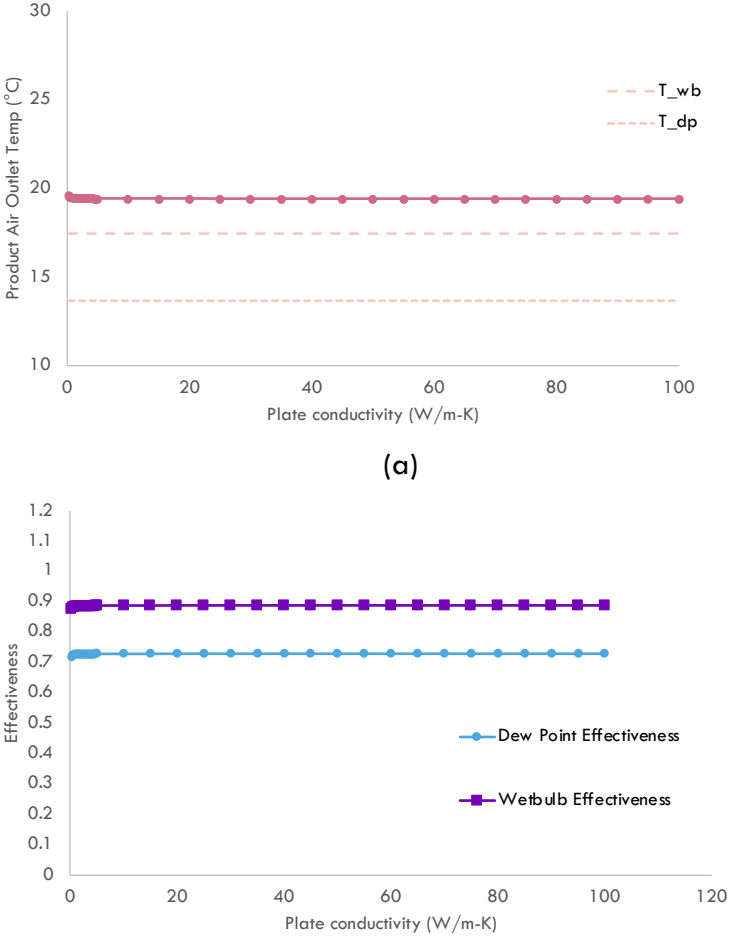


Figure 23: Effect of plate conductivity

The parametric analysis showed that primary side air flow rate, channel lengths of both the primary and secondary side and primary channel height had the most impact on the performance metrics. The dew-point and wet-bulb effectiveness showed higher values at primary air flow rates of around 0.35 m<sup>3</sup>/s. However, the heat transferred showed the

opposite trend- it increased with an increase in air flow rate. An optimum range would be between 0.45-0.5 m<sup>3</sup>/s with reasonably good dew-point and wet-bulb effectiveness and heat transferred.

The secondary air flow rate did not significantly impact the performance parameters.

While the performance parameters improved drastically with increasing channel lengths on primary side, the pressure drop also increased linearly. In case of secondary channel length, the performance metrics improved initially and reached a stagnation at longer channel lengths although in case too, there was a linear increase in pressure drop. The recommended channel lengths would thus be between 0.4- 0.6 m on the primary side and between 0.15- 0.25 m on the secondary side. Since secondary channel length has been defined as function of number of primary channels, this would correspond to primary channels between 5 and 10 on the primary side (in half core).

Increasing the channel heights on both sides deteriorated the performance metrics. However, a smaller height necessitated higher pumping power – there was a steep increase below 0.003 m on primary side and 0.004 m on secondary side. These values would be optimum to achieve a good performance while also saving up on the pumping power.

## CONCLUSION AND SCOPE FOR FUTURE WORK

Based on heat and mass transfer principles, a numerical model of an indirect evaporative cooling system was developed. The system's performance was projected using the model's known inlet parameters. For varied inlet air conditions, the modeling results were compared to the experimental data. Within a 10% variance in the outlet air temperature, there was good agreement and trend between simulation and experimental results. The mean average errors (MAE) reduced for the primary outlet temperatures, secondary outlet temperatures and humidity ratios were 0.78 °C, 1.22°C and 0.0007 respectively.

Furthermore, a parametric study was conducted to determine the effect of several parameters on cooling performance, namely the product air outlet temperature, wet-bulb effectiveness, and dew-point effectiveness. The parameters under consideration were namely airflow rate, channel length, height, plate thickness and plate conductivity. Some of the observations consistent with reviewed literature are:

- The product air intake velocity must be small for a higher cooling effectiveness.
- Optimum channel height should be around 5 mm on both sides.
- Longer channel length on the product side gives better cooling performance. The trade-off with pressure drop needs to be accounted for while increasing channel length.
- The contribution of plate thermal conductivity is negligible to the system cooling performance.

For simplification of computation within the time frame, only test cases without condensation on the primary side were considered for the sake of modeling and verification. It would be



worthwhile to assess the cases with condensation and develop a model that accounts for the same.

## NOMENCLATURE

$A_{finned}$	= Finned heat transfer area (m <sup>2</sup> )
$A_{unfinned}$	= Un-finned heat transfer area (m <sup>2</sup> )
$A_{plate}$	= Area of separation plate between dry and wet channels (m <sup>2</sup> )
$A_c$	= Area of cross section (m <sup>2</sup> )
$A_{total}$	= Total heat transfer area (m <sup>2</sup> )
$c_p$	= Specific heat (J/kg-K)
$d_0$	= Hole diameter on separation plate (m)
$d_{water-air}$	= Diffusion coefficient of water in air (m <sup>2</sup> /s)
$f$	= Fractional fiber ratio (fraction of wet surface covered by wicking fiber)
$g_m$	= Mass Transfer Conductance (kg/m <sup>2</sup> -s)
$h$	= Specific Enthalpy (J/kg)
$h_f$	= Fin height (m)
$h_{vap}$	= Enthalpy of vaporization (J/kg)
$htc$	= Heat transfer coefficient (W/m <sup>2</sup> -K)
$H$	= Height of the channel (m)
$i$	= Counting index along x-direction
$j$	= Counting index along y-direction
$k$	= Thermal conductivity (W/m-K)
$l_f$	= Fin length (m)
$L$	= Length of channel (m)

$M_{air}$	= Molar mass of air (kg/kmol)
$m_f$	= Mass fraction
$M_{water}$	= Molar mass of water (kg/kmol)
$\dot{m}$	= Mass flow rate (kg/s)
$M$	= Number of sub-divisions on primary side
$N$	= Number of sub-divisions on secondary side
$N_{ch}$	= Number of channels
$N_{core}$	= Number of cores in the HMX
$N_{rows}$	= Number of rows in a core
$N_{sections}$	= Number of sections in a core
$Nusselt$	= Nusselt number
$pe$	= Perimeter (m)
$P$	= Pressure (Pa)
$Q$	= Heat transferred (W)
$R$	= Resistance (K/W)
$Re$	= Reynold's number
$RelRough$	= Relative roughness of channel
$Sc$	= Schmidt number
$Sh$	= Sherwood number
$T$	= Temperature (K)

$v$	= Velocity (m/s)
$\dot{V}$	= Volume flow rate (m <sup>3</sup> /s)
$w_f$	= Fin width (m)
$W$	= Width of channel (m)
$x_f$	= Mole fraction

#### Greek Symbols

$\delta$	= Thickness (m)
$\varepsilon$	= Effectiveness
$\eta$	= Efficiency
$\nu$	= Kinematic viscosity (m <sup>2</sup> /s)
$\rho$	= Density (kg/m <sup>3</sup> )
$\omega$	= Humidity ratio

#### Subscripts

<i>atm</i>	= Attributed to atmospheric condition
<i>avg</i>	= Average
<i>bottom</i>	= Attributed to bottom (secondary) channel
<i>cond</i>	= Attributed to conduction heat transfer
<i>ch</i>	= Attributed to a channel

<i>dp</i>	= Dewpoint
<i>f</i>	= Attributed to fin
<i>fiber</i>	= Attributed to fiber
<i>firsthalf</i>	= Attributed to first half (containing 10 holes) of channel 1 on top
<i>halfcore</i>	= Attributed to one half of the core/ one section
<i>in</i>	= Calculated at inlet
<i>l</i>	= Latent
<i>min</i>	= Minimum value
<i>o/out</i>	= Calculated at outlet
<i>p</i>	= Attributed to primary side
<i>plate</i>	= Attributed to separation plate
<i>s</i>	= Attributed to secondary side
<i>sat</i>	= Attributed to saturation condition
<i>secondhalf</i>	= Attributed to second half (containing 10 holes) of channel 1 on top
<i>top</i>	= Attributed to first channel on top with holes
<i>total</i>	= Total
<i>wall</i>	= Calculated at wall
<i>water</i>	= Attributed to water
<i>wb</i>	= Wet-bulb

## Acronyms

CCU	= Cooling Coil Unit
COP	= Coefficient Of Performance
DEC	= Direct Evaporative cooler
DPD	= Dew Point Desalination
EC	= Evaporative Cooling
EES	= Engineering Equation Solver
ERV	= Energy Recovery Ventilator
GCC	= Ground Coupled Circuit
GWP	= Global Warming Potential
HDH	= Humidification- Dehumidification
HMX	= Heat and Mass Exchanger
HVAC	= Heating, Ventilation and Air-Conditioning
IEC	= Indirect Evaporative Cooler
MAE	= Mean Average Error
PAT	= Primary Approach Temperature
SAT	= Secondary Approach Temperature
WBT	= Wet-Bulb Temperature

## REFERENCES

- [1] Zhan, C., Zhao, X., Smith, S., & Riffat, S. (2011). Numerical study of a M-cycle crossflow heat exchanger for indirect evaporative cooling. *Fuel and Energy Abstracts*.
- [2] Wu, X., Hu, S., & Mo, S. (2013). Carbon footprint model for evaluating the global warming impact of food transport refrigeration systems. *Journal of Cleaner Production*, 54, 115-124.
- [3] O'Connor, D., Calautit, J.K., & Hughes, B.R. (2016). A review of heat recovery technology for passive ventilation applications. *Renewable & Sustainable Energy Reviews*, 54, 1481-1493.
- [4] Cuce, P.M., & Riffat, S. (2016). A state-of-the-art review of evaporative cooling systems for building applications. *Renewable & Sustainable Energy Reviews*, 54, 1240-1249.
- [5] Chu, J., & Huang, X. (2021). Research status and development trends of evaporative cooling air-conditioning technology in data centers. *Energy and Built Environment*.
- [6] Sethi, V.P., & Sharma, S.K. (2007). Survey of cooling technologies for worldwide agricultural greenhouse applications. *Solar Energy*, 81, 1447-1459.
- [7] Ndukaife, T.A., & Nnanna, A.G. (2019). Optimization of Water Consumption in Hybrid Evaporative Cooling Air Conditioning Systems for Data Center Cooling Applications. *Heat Transfer Engineering*, 40, 559 - 573.
- [8] Pandelidis, D., Cichoń, A., Pacak, A., Drąg, P., Drąg, M., Worek, W., & Cetin, S. (2021). Water desalination through the dewpoint evaporative system. *Energy Conversion and Management*, 229, 113757.
- [9] Raza, H. M., Sultan, M., Bahrami, M., & Khan, A. A. (2021). Experimental investigation of evaporative cooling systems for agricultural storage and livestock air-conditioning in Pakistan. In *Building Simulation* (Vol. 14, No. 3, pp. 617-631). Tsinghua University Press.
- [10] Costelloea, B., & Finn, D. (2020). Indirect Evaporative Cooling Potential in Air-water Systems in Temperate Climates.

- [11] Ebrahim Hajidavalloo (2007). Application of evaporative cooling on the condenser of window-air-conditioner, *Applied Thermal Engineering*, 27, 1937-1943.
- [12] Krarti, M. (2018). *Integrated Design and Retrofit of Buildings*, Chapter 6, 313-384.
- [13] Porumb, B., Ungureşan, P., Tutunaru, L.F., Şerban, A., & Balan, M.C. (2016). A Review of Indirect Evaporative Cooling Technology. *Energy Procedia*, 85, 461-471.
- [14] Maisotsenko, V., Gillan, L.E., Heaton, T.L., Gillan, A.D., 2002. Method and apparatus of indirect-evaporation cooling. US6497107 B2 Patent.
- [15] Mahmood, M.H., Sultan, M., Miyazaki, T., Koyama, S., & Maisotsenko, V.S. (2016). Overview of the Maisotsenko cycle – A way towards dew point evaporative cooling. *Renewable & Sustainable Energy Reviews*, 66, 537-555.
- [16] Pandelidis, D., & Anisimov, S. (2015). Numerical analysis of the heat and mass transfer processes in selected M-Cycle heat exchangers for the dew point evaporative cooling. *Energy Conversion and Management*, 90, 62-83.
- [17] Riangvilaikul, B., & Kumar, S. (2010). An experimental study of a novel dew point evaporative cooling system. *Energy and Buildings*, 42, 637-644.
- [18] Chua, K.J., Chou, S.K., Yang, W., & Yan, J. (2013). Achieving better energy-efficient air conditioning - A review of technologies and strategies. *Applied Energy*, 104, 87-104.
- [19] Pandelidis, D., Anisimov, S., & Worek, W.M. (2015). Performance study of the Maisotsenko Cycle heat exchangers in different air-conditioning applications. *International Journal of Heat and Mass Transfer*, 81, 207-221.
- [20] Coolerado Corporation, 4430 Glencoe St. Denver, CO 80216, USA. <http://www.coolerado.com/> ; 2015.
- [21] Coolerado cooler helps to save cooling energy and dollars: new cooling technology targets peak load reduction. United States: U. S. Department of Energy, Energy Efficiency & Renewable



Energy, Federal Energy Management Program (FEMP), Report no. DOE/GO-102007-2325, ≤ <http://www.osti.gov/scitech/biblio/908968>> ; 2007.

[22] Moshari, S., Heidarinejad, G., & Fathipour, A. (2016). Numerical investigation of wet-bulb effectiveness and water consumption in one-and two-stage indirect evaporative coolers. *Energy Conversion and Management*, 108, 309-321.

[23] Al Horr, Y., Tashtoush, B., Chilengwe, N., & Musthafa, M.M. (2020). Operational mode optimization of indirect evaporative cooling in hot climates. *Case Studies in Thermal Engineering*, 18, 100574.

[24] Amer, O.M., Boukhanouf, R., & Ibrahim, H.G. (2014). A Review of Evaporative Cooling Technologies.

[25] Cuce, P.M., & Riffat, S. (2016). A state-of-the-art review of evaporative cooling systems for building applications. *Renewable & Sustainable Energy Reviews*, 54, 1240-1249.

[26] Basediya, A.L., Samuel, D.V., & Beera, V. (2011). Evaporative cooling system for storage of fruits and vegetables - a review. *Journal of Food Science and Technology*, 50, 429-442.

[27] Yang, Y., Cui, G., & Lan, C.Q. (2019). Developments in evaporative cooling and enhanced evaporative cooling - A review. *Renewable and Sustainable Energy Reviews*.

[28] Rafique, M.M., Gandhidasan, P., Rehman, S., & Al-Hadhrami, L.M. (2015). A review on desiccant based evaporative cooling systems. *Renewable & Sustainable Energy Reviews*, 45, 145-159.

[29] Rampazzo, M., Lionello, M., Beghi, A., Sisti, E., & Cecchinato, L. (2019). A static moving boundary modelling approach for simulation of indirect evaporative free cooling systems. *Applied Energy*.

[30] Pandelidis, D., Cichoń, A., Pacak, A., Anisimov, S., & Drąg, P. (2018). Counter-flow indirect evaporative cooler for heat recovery in the temperate climate. *Energy*.

- [31] Hao, J., Chen, Q., Li, X., Zhang, M., & Yuan, F. (2019). A new modeling and analysis method of the indirect evaporative heat exchanger based on the heat current perspective. *Applied Thermal Engineering*, 163, 114331.
- [32] Wang, Y., Huang, X., & Li, L. (2018). Comparative Study of the Cross-Flow Heat and Mass Exchangers for Indirect Evaporative Cooling Using Numerical Methods. *Energies*.
- [33] Guo, C., Liu, Q., Zheng, B., You, Y., & Li, Y. (2020). Development of model based on condensation area ratio and effect on heat transfer capacity of indirect evaporative cooling. *Applied Thermal Engineering*, 164, 114557.
- [34] Wan, Y., Soh, A., Shao, Y.L., Cui, X., Tang, Y., & Chua, K.J. (2020). Numerical study and correlations for heat and mass transfer coefficients in indirect evaporative coolers with condensation based on orthogonal test and CFD approach. *International Journal of Heat and Mass Transfer*, 153, 119580.
- [35] Bruno, F. (2011). On-site experimental testing of a novel dew point evaporative cooler. *The Lancet*.
- [36] Zhan, C., Duan, Z., Zhao, X., Smith, S., Jin, H., & Riffat, S. (2011). Comparative study of the performance of the M-cycle counter-flow and cross-flow heat exchangers for indirect evaporative cooling – Paving the path toward sustainable cooling of buildings. *Energy*, 36, 6790-6805.
- [37] Guo, X.C., & Zhao, T. (1998). A parametric study of an indirect evaporative air cooler. *International Communications in Heat and Mass Transfer*, 25, 217-226.
- [38] Khalid, O., Ali, M., Sheikh, N.A., Ali, H.M., & Shehryar, M. (2016). Experimental analysis of an improved Maisotsenko cycle design under low velocity conditions. *Applied Thermal Engineering*, 95, 288-295.
- [39] Duan, Z., Zhan, C., Zhao, X., & Dong, X. (2016). Experimental study of a counter-flow regenerative evaporative cooler. *Building and Environment*, 104, 47-58.

- [40] Zhao, X., Li, J., & Riffat, S. (2008). Numerical study of a novel counter-flow heat and mass exchanger for dew point evaporative cooling. *Applied Thermal Engineering*, 28, 1942-1951.
- [41] Khalid, O., Butt, Z., Tanveer, W.H., & Rao, H.I. (2017). Design and experimental analysis of counter-flow heat and mass exchanger incorporating (M-cycle) for evaporative cooling. *Heat and Mass Transfer*, 53, 1391-1403.
- [42] Xu, P., Ma, X., Diallo, T.M., Zhao, X., Fancey, K.S., Li, D., & Chen, H. (2016). Numerical investigation of the energy performance of a guideless irregular heat and mass exchanger with corrugated heat transfer surface for dew point cooling. *Energy*, 109, 803-817.
- [43] Cui, X., Chua, K.J., & Yang, W. (2014). Numerical simulation of a novel energy-efficient dew-point evaporative air cooler. *Applied Energy*, 136, 979-988.
- [44] Anisimov, S., & Pandelidis, D. (2014). Numerical study of the Maisotsenko cycle heat and mass exchanger. *International Journal of Heat and Mass Transfer*, 75, 75-96.
- [45] Pandelidis, D., Anisimov, S., & Worek, W.M. (2015). Comparison study of the counter-flow regenerative evaporative heat exchangers with numerical methods. *Applied Thermal Engineering*, 84, 211-224.
- [46] Kim, N. (2016). Heat and moisture transfer in a counter flow regenerative evaporative cooler made of plastic film/paper composite. *Journal of Mechanical Science and Technology*, 30, 1449-1457.
- [47] Fikri, B., Sofia, E., & Putra, N. (2020). Experimental analysis of a multistage direct-indirect evaporative cooler using a straight heat pipe. *Applied Thermal Engineering*, 171, 115133.
- [48] Matsui, K., Thu, K., & Miyazaki, T. (2020). A hybrid power cycle using an inverted Brayton cycle with an indirect evaporative device for waste-heat recovery. *Applied Thermal Engineering*, 170, 115029.

- [49] Comino, F., Adana, M.R., & Peci, F. (2018). Energy saving potential of a hybrid HVAC system with a desiccant wheel activated at low temperatures and an indirect evaporative cooler in handling air in buildings with high latent loads. *Applied Thermal Engineering*, 131, 412-427.
- [50] Khalajzadeh, V., Farmahini-Farahani, M., & Heidarinejad, G. (2012). A novel integrated system of ground heat exchanger and indirect evaporative cooler. *Energy and Buildings*, 49, 604-610.
- [51] Chen, Q., Burhan, M., Shahzad, M.W., Ybyraiymkul, D., Akhtar, F.H., & Ng, K.C. (2020). Simultaneous production of cooling and freshwater by an integrated indirect evaporative cooling and humidification-dehumidification desalination cycle. *Energy Conversion and Management*, 221, 113169.
- [52] Wu, J., Xiang, H., & Zhang, H. (2009). Numerical investigation on the heat and mass transfer in a direct evaporative cooler. *Applied Thermal Engineering*, 29, 195-201.
- [53] Taler, J., Jagieła, B., & Jaremkiewicz, M. (2022). Overview of the M-Cycle Technology for Air Conditioning and Cooling Applications. *Energies*.
- [54] Adam, A., Han, D., He, W., Amidpour, M., & Zhong, H. (2022). Numerical investigation of the heat and mass transfer process within a cross-flow indirect evaporative cooling system for hot and humid climates. *Journal of Building Engineering*.
- [55] Talukdar, P., Olutmayin, S.O., Osanyintola, O.F., & Simonson, C.J. (2007). An experimental data set for benchmarking 1-D, transient heat and moisture transfer models of hygroscopic building materials. Part I: Experimental facility and material property data. *International Journal of Heat and Mass Transfer*, 50, 4527-4539.
- [56] Riffat, S., & Gan, G. (1998). Determination of effectiveness of heat-pipe heat recovery for naturally-ventilated buildings. *Applied Thermal Engineering*, 18, 121-130.
- [57] Xu, Q., Riffat, S., & Zhang, S. (2019). Review of Heat Recovery Technologies for Building Applications. *Energies*.

- [58] Gendebien, S., Parthoens, A., & Lemort, V. (2019). Investigation of a single room ventilation heat recovery exchanger under frosting conditions: Modeling, experimental validation and operating strategies evaluation. *Energy and Buildings*.
- [59] Yaïci, W., Ghorab, M.G., & Entchev, E. (2013). Numerical analysis of heat and energy recovery ventilators performance based on CFD for detailed design. *Applied Thermal Engineering*, 51, 770-780.
- [60] Li, J., Zmeureanu, R., & Ge, H. (2021). Modeling the effect of dual-core energy recovery ventilator unit on the energy use of houses in northern Canada. *Applied Thermal Engineering*.
- [61] Mardiana, A., & Riffat, S. (2013). Review on physical and performance parameters of heat recovery systems for building applications. *Renewable & Sustainable Energy Reviews*, 28, 174-190.
- [62] Chen, X., Su, Y., Reay, D.A., & Riffat, S. (2016). Recent research developments in polymer heat exchangers – A review. *Renewable & Sustainable Energy Reviews*, 60, 1367-1386.
- [63] Nasif, M.S. (2015). Effect of utilizing different permeable material in air to air fixed plate energy recovery heat exchanger on energy saving.
- [64] Li, W., Li, Y., Zeng, L., & Lu, J. (2018). Comparative study of vertical and horizontal indirect evaporative cooling heat recovery exchangers. *International Journal of Heat and Mass Transfer*.
- [65] Li, J., Zmeureanu, R., & Ge, H. (2021). Modeling the effect of dual-core energy recovery ventilator unit on the energy use of houses in northern Canada. *Applied Thermal Engineering*.
- [66] 6B Coolerado HMX Bro US-0516 - Seeley International. (n.d.). Seeley International.  
[https://www.seeleyinternational.com/us/artefact/6b\\_coolerado-hmx-bro\\_us-0516/](https://www.seeleyinternational.com/us/artefact/6b_coolerado-hmx-bro_us-0516/)

## APPENDIX

Detailed list of equations

### A. Primary Channel Inputs

$$N_{chp_{core}} = N_{rows} * N_{chp_{halfrow}} * N_{sections}$$

$$N_{ch_{top_{core}}} = N_{rows} * N_{sections}$$

$$N_{p_{total}} = N_{core} * N_{chp_{core}}$$

$$\dot{V}_{in_p} = \frac{\dot{V}_{p_{total}}}{N_{p_{total}}}$$

$$v_{in_p} = \frac{\dot{V}_{in_p}}{H_p * W_p}$$

$$\dot{m}_{in_{p_{ch}}} = \frac{\dot{V}_{in_p}}{\rho_{in_p}}$$

$$c_{p_{in_p}} = cp(AirH2O, T = T_{in_p}, \omega = \omega_{in_p}, P = P_{in_p})$$

$$\rho_{in_p} = density(AirH2O, T = T_{in_p}, \omega = \omega_{in_p}, P = P_{in_p})$$

$$h_{in_p} = enthalpy(AirH2O, T = T_{in_p}, \omega = \omega_{in_p}, P = P_{in_p})$$

$$Call\ ductflow \left( \begin{array}{l} 'AirH2O', T_{in_p}, P_{in_p}, \dot{m}_{in_{p_{ch}}}, H_p, W_p, L, \\ RelRough_p: htc_{T_p}, htc_{H_p}, \Delta P_p, Nusselt_{T_p}, Re_p \end{array} \right)$$

$$htc_p = \frac{htc_{T_p} + htc_{H_p}}{2}$$

### B. Secondary Channel Inputs

$$T_{in_{s_{dp}}} = dewpoint(AirH2O, T = T_{in_s}, \omega = \omega_{in_s}, P = P_{in_s})$$

$$T_{in_{s_{wb}}} = wetbulb(AirH2O, T = T_{in_s}, \omega = \omega_{in_s}, P = P_{in_s})$$

$$c_{p_{in_s}} = cp(AirH2O, T = T_{in_s}, \omega = \omega_{in_s}, P = P_{in_s})$$

$$\rho_{in_s} = density(AirH2O, T = T_{in_s}, \omega = \omega_{in_s}, P = P_{in_s})$$

$$h_{in_s} = enthalpy(AirH2O, T = T_{in_s}, \omega = \omega_{in_s}, P = P_{in_s})$$

$$Call\ ductflow \left( \begin{array}{l} 'AirH2O', T_{in_s}, P_{in_s}, \dot{m}_{in_{s_{ch}}}, H_s, W_s, L, \\ RelRough_s: htc_{T_s}, htc_{H_s}, \Delta P_s, Nusselt_{T_s}, Re_s \end{array} \right)$$

$$htc_s = \frac{htc_{T_s} + htc_{H_s}}{2}$$

### C. Inputs to top section with holes

$$\begin{aligned}
N_{top\_total} &= N_{core} * N_{ch\_top\_core} \\
W_{top\_ch} &= W_p * N_{ch\_stophalfrow} \\
\dot{V}_{top} &= \frac{\dot{V}_{stotal}}{N_{top\_total}} \\
v_{in\_top} &= \frac{\dot{V}_{top}}{H_p * W_{top\_ch}} \\
\dot{m}_{in\_top} &= \frac{\dot{V}_{top}}{\rho_{in\_top}} \\
\rho_{in\_top} &= \text{density}(\text{AirH2O}, T = T_{in_s}, \omega = \omega_{in_s}, P = P_{in_s})
\end{aligned}$$

#### D. Fin Calculations

$$\begin{aligned}
A_{finned_p} &= N_{ch\_phalfrow} (2l_{f_p} h_{f_p}) \\
A_{finned_s} &= N_{ch\_sbottomhalfrow} (2l_{f_s} h_{f_s}) \\
A_{plate} &= (N_{ch\_phalfrow} W + (N_{ch\_phalfrow} + 1)w_f)(L + w_f) \\
A_{unfinned_p} &= A_{plate} - (N_{ch\_phalfrow} + 1)l_{f_p} w_f \\
A_{unfinned_s} &= A_{plate} - (N_{ch\_sbottomhalfrow} + 1)l_{f_s} w_f \\
A_{c_p} &= l_{f_p} w_f \\
pe_p &= 2l_{f_p} + w_f \\
A_{c_s} &= l_{f_s} w_f \\
pe_s &= 2l_{f_s} + w_f \\
\eta_{f_p} &= \text{eta\_fin\_constantcs}(A_{c_p}, pe_p, h_{f_p}, htc_p, k_{plate}) \\
\eta_{f_s} &= \text{eta\_fin\_constantcs}(A_{c_s}, pe_s, h_{f_s}, htc_s, k_{plate}) \\
A_{total_p} &= (A_{finned_p} * \eta_{f_p}) + A_{unfinned_p} \\
A_{total_s} &= (A_{finned_s} * \eta_{f_s}) + A_{unfinned_s}
\end{aligned}$$

#### E. Resistance Calculations

$$\begin{aligned}
R_p &= \frac{1}{htc_p * \frac{A_{total_p}}{(M-1)N}} \\
R_{plate} &= \frac{\delta_{plate}}{k_{plate} * \frac{A_{plate}}{(M-1)N}}
\end{aligned}$$

$$R_{fiber} = \frac{\delta_{fiber}}{k_{fiber} * \frac{A_{plate} * f}{(M-1)N}}$$

$$R_{water} = \frac{\delta_{fiber}}{k_{water} * \frac{A_{plate} * (1-f)}{(M-1)N}}$$

$$R_{cond} = R_{plate} + \frac{R_{fiber}R_{water}}{R_{fiber} + R_{water}}$$

$$R_{total} = R_{cond} + R_p$$

F. Heat transfer calculation between channel (i=)2 to 6 on primary side and (j=) 1 to 20 on secondary side

i. Boundary Conditions

$$T_p[i, 1] = T_{in_p}; i: 2 \text{ to } M$$

$$h_p[i, 1] = h_{in_p}; i: 2 \text{ to } M$$

ii. Mass Transfer Conductance

$$\rho_s[i, j] = \mathbf{density}(\mathbf{AirH2O}, T = T_s[i, j], \omega = \omega_s[i, j], \mathbf{P} = P_{in_s})$$

$$v_s[i, j] = \mathbf{kinematicviscosity}(\mathbf{AirH2O}, T = T_s[i, j], \omega = \omega_s[i, j], \mathbf{P} = P_{in_s})$$

$$d_{water-air}[i, j] = 1.97 * 10^{-5} \frac{P_{atm}}{P_{in_s}} \left( \frac{T_s[i, j]}{T_0} \right)^{1.685}$$

$$Sc[i, j] = \frac{v_s[i, j]}{d_{water-air}[i, j]}$$

$$g_{m_{water}}[i, j] = \frac{\rho_s[i, j] * v_s[i, j] * Sh}{Sc[i, j] * 2H_s}$$

iii. Mass fraction

$$P_{sat}[i, j] = \mathbf{p\_sat}(\mathbf{Water}, T = T_{wall}[i, j])$$

$$x_{f_{wall}}[i, j] = \frac{P_{sat}[i, j]}{P_{atm}}$$

$$m_{f_{wall}}[i, j] = \frac{x_{f_{wall}}[i, j] * m_{water}}{x_{f_{wall}}[i, j]m_{water} + (1 - x_{f_{wall}}[i, j])m_{air}}$$

$$m_f[i + 1, j] = \frac{\omega_s[i + 1, j]}{\omega_s[i + 1, j] + 1}$$



$$\begin{aligned}
m_{f_{avg}}[i,j] &= \frac{m_f[i,j] + m_f[i+1,j]}{2} \\
\frac{m_{s_{bottomch}}}{2} (m_f[i+1,j] - m_f[i,j]) \\
&= g_{m_{water}}[i,j] * (m_{f_{wall}}[i,j] - m_{f_{avg}}[i,j]) \\
&\quad * \frac{A_{unfinned_s}}{(M-1) * N}
\end{aligned}$$

iv. Dry channel energy balance

$$\begin{aligned}
T_{p_{avg}}[i,j] &= \frac{T_p[i,j] + T_p[i,j+1]}{2} \\
h_p[i,j+1] &= \mathbf{enthalpy}(\mathbf{AirH2O}, T = T_p[i,j+1], \boldsymbol{\omega} = \boldsymbol{\omega}_{in_p}, \mathbf{P} = P_{in_p}) \\
Q_p[i,j] &= \frac{1}{R_{total}} * (T_{p_{avg}}[i,j] - T_{wall}[i,j]) \\
Q_p[i,j] &= \frac{\dot{m}_{in_pch}}{2} * (h_p[i,j] - h_p[i,j+1])
\end{aligned}$$

v. Wet channel energy balance

$$\begin{aligned}
T_{s_{avg}}[i,j] &= \frac{T_s[i,j] + T_s[i+1,j]}{2} \\
h_s[i+1,j] &= \mathbf{enthalpy}(\mathbf{AirH2O}, T = T_s[i+1,j], \boldsymbol{\omega} = \boldsymbol{\omega}_s[i+1,j], \mathbf{P} = P_{in_s}) \\
Q_p[i,j] &= \frac{\dot{m}_{s_{bottomch}}}{2} * (h_s[i+1,j] - h_s[i,j]) \\
Q_s[i,j] &= \frac{htc_s}{2} * (T_{wall}[i,j] - T_{s_{avg}}[i,j]) * \frac{A_{total_s}}{(M-1) * N} \\
Q_i[i,j] &= g_{m_w}[i,j] * (m_{f_{wall}}[i,j] - m_{f_{avg}}[i,j]) * \Delta h_{vap}[i,j] * \frac{A_{unfinned_s}}{(M-1) * N} \\
Q_p[i,j] &= Q_i[i,j] + Q_s[i,j] \\
\Delta h_{vap}[i,j] &= \mathbf{enthalpy\_vaporization}(\mathbf{Water}, T = T_{wall}[i,j])
\end{aligned}$$

G. Heat transfer calculation for top channel

i. Boundary conditions

$$\begin{aligned}
 T_p[1,1] &= T_{in_s} \\
 h_p[1,1] &= h_{in_s} \\
 \dot{m}_{top}[1,1] &= \dot{m}_{in_{top}} \\
 \dot{m}_{s_{bottomch}} &= \frac{\dot{m}_{in_{top}}}{N} \\
 \omega_s[1,j] &= \omega_{in_s}; j: 1 \text{ to } N \\
 m_f[1,j] &= \frac{\omega_{in_s}}{\omega_{sin} + 1}; j: 1 \text{ to } N
 \end{aligned}$$

ii. Area calculations

$$\begin{aligned}
 A_{plate_{firsthalf}} &= \frac{l_{fp}}{2} * W_{topch} - \left( \frac{N}{2} * \pi * \frac{d_0^2}{4} \right) \\
 A_{plate_{secondhalf}} &= \frac{l_{fp}}{2} * (W_{topch} - W_p) - \left( \frac{N}{2} * \pi * \frac{d_0^2}{4} \right)
 \end{aligned}$$

H. Heat transfer calculation for top channel (first half with 10 holes; j: 1 to N/2)

i. Boundary Conditions

$$\begin{aligned}
 T_{p_{avg}}[1,j] &= \frac{T_p[1,j] + T_p[1,j+1]}{2} \\
 T_s[1,j] &= T_{p_{avg}}[1,j] \\
 h_s[1,j] &= \mathbf{enthalpy}(\mathbf{AirH2O}, \mathbf{T} = T_s[1,j], \boldsymbol{\omega} = \omega_s[1,j], \mathbf{P} = P_{in_s}) \\
 \dot{m}_{top}[1,j+1] &= \dot{m}_{top}[1,j] - \dot{m}_{s_{bottomch}}
 \end{aligned}$$

ii. Mass Transfer Conductance

$$\begin{aligned}
 \rho_s[1,j] &= \mathbf{density}(\mathbf{AirH2O}, \mathbf{T} = T_s[1,j], \boldsymbol{\omega} = \omega_s[1,j], \mathbf{P} = P_{in_s}) \\
 \nu_s[1,j] &= \mathbf{kinematicviscosity}(\mathbf{AirH2O}, \mathbf{T} = T_s[1,j], \boldsymbol{\omega} = \omega_s[1,j], \mathbf{P} = P_{in_s}) \\
 d_{water-air}[1,j] &= 1.97 * 10^{-5} \frac{P_{atm}}{P_{in_s}} \left( \frac{T_s[1,j]}{T_0} \right)^{1.685} \\
 Sc[1,j] &= \frac{\nu_s[1,j]}{d_{water-air}[1,j]}
 \end{aligned}$$

$$g_{m_{water}}[1,j] = \frac{\rho_s[1,j] * v_s[1,j] * Sh}{Sc[1,j] * 2H_s}$$

iii. Mass fraction

$$\begin{aligned}
P_{sat}[1,j] &= \mathbf{p\_sat}(\mathbf{Water}, T = T_{wall}[1,j]) \\
x_{f_{wall}}[1,j] &= \frac{P_{sat}[1,j]}{P_{atm}} \\
m_{f_{wall}}[1,j] &= \frac{x_{f_{wall}}[1,j] * m_{water}}{x_{f_{wall}}[1,j]m_{water} + (1 - x_{f_{wall}}[1,j])m_{air}} \\
m_f[2,j] &= \frac{\omega_s[2,j]}{\omega_s[2,j] + 1} \\
m_{f_{avg}}[1,j] &= \frac{m_f[1,j] + m_f[2,j]}{2} \\
\frac{m_{s_{bottomch}}}{2} (m_f[2,j] - m_f[1,j]) &= g_{m_{water}}[1,j] * (m_{f_{wall}}[1,j] - m_{f_{avg}}[1,j]) \\
&* \frac{2 * A_{platefirsthalf}}{N}
\end{aligned}$$

iv. Top channel energy balance

$$\begin{aligned}
\mathbf{Call\ ductflow} &\left( \begin{array}{l} 'AirH2O', T_{p_{avg}}[1,j], P_{ins}, \dot{m}_{top}[1,j], H_p, W_{topch}, \frac{l_{fp}}{2}, \\ RelRough_p, htc_{T_{top}}[1,j], htc_{H_{top}}[1,j], \Delta P_{top}[1,j], \\ Nusselt_{top}[1,j], f_{top}[1,j], Re_{top}[1,j] \end{array} \right) \\
htc_{top}[1,j] &= \frac{htc_{T_{top}}[1,j] + htc_{H_{top}}[1,j]}{2} \\
h_p[1,j + 1] &= \mathbf{enthalpy}(\mathbf{AirH2O}, T = T_p[1,j + 1], \omega = \omega_s[1,j], P = P_{ins}) \\
Q_p[1,j] &= htc_{top}[1,j] * (T_{p_{avg}}[i,j] - T_{wall}[i,j]) * \frac{2 * A_{platefirsthalf}}{N} \\
Q_p[1,j] &= \frac{\dot{m}_{top}[1,j]}{2} * h_p[1,j] - \frac{\dot{m}_{top}[1,j + 1]}{2} * h_p[1,j + 1] - \frac{m_{s_{bottomch}}}{2} \\
&* h_s[1,j]
\end{aligned}$$

v. Wet channel energy balance

$$T_{s_{avg}}[1,j] = \frac{T_s[1,j] + T_s[2,j]}{2}$$

$$h_s[2,j] = \mathbf{enthalpy}(\mathbf{AirH2O}, T = T_s[2,j], \boldsymbol{\omega} = \boldsymbol{\omega}_s[2,j], \mathbf{P} = P_{in_s})$$

$$Q_p[1,j] = \frac{\dot{m}_{s_{bottomch}}}{2} * (h_s[2,j] - h_s[1,j])$$

$$Q_s[1,j] = \frac{htc_s}{2} * (T_{wall}[1,j] - T_{s_{avg}}[1,j]) * \frac{2 * A_{plate_{firsthalf}}}{N}$$

$$Q_l[1,j] = g_{m_w}[1,j] * (m_{f_{wall}}[1,j] - m_{f_{avg}}[1,j]) * \Delta h_{vap}[1,j] * \frac{2 * A_{plate_{firsthalf}}}{N}$$

$$Q_p[1,j] = Q_l[1,j] + Q_s[1,j]$$

$$\Delta h_{vap}[i,j] = \mathbf{enthalpy\_vaporization}(\mathbf{Water}, T = T_{wall}[1,j])$$

i. Heat transfer calculation for top channel (second half with 10 holes; j: N/2 + 1 to N)

i. Boundary Conditions

$$T_{p_{avg}}[1,j] = \frac{T_p[1,j] + T_p[1,j+1]}{2}$$

$$T_s[1,j] = T_{p_{avg}}[1,j]$$

$$h_s[1,j] = \mathbf{enthalpy}(\mathbf{AirH2O}, T = T_s[1,j], \boldsymbol{\omega} = \boldsymbol{\omega}_s[1,j], \mathbf{P} = P_{in_s})$$

$$m_{top}[1,j+1] = m_{top}[1,j] - \dot{m}_{s_{bottomch}}$$

ii. Mass Transfer Conductance

$$\rho_s[1,j] = \mathbf{density}(\mathbf{AirH2O}, T = T_s[1,j], \boldsymbol{\omega} = \boldsymbol{\omega}_s[1,j], \mathbf{P} = P_{in_s})$$

$$\nu_s[1,j] = \mathbf{kinematicviscosity}(\mathbf{AirH2O}, T = T_s[1,j], \boldsymbol{\omega} = \boldsymbol{\omega}_s[1,j], \mathbf{P} = P_{in_s})$$

$$d_{water-air}[1,j] = 1.97 * 10^{-5} \frac{P_{atm}}{P_{in_s}} \left( \frac{T_s[1,j]}{T_0} \right)^{1.685}$$

$$Sc[1,j] = \frac{\nu_s[1,j]}{d_{water-air}[1,j]}$$

$$g_{m_{water}}[1,j] = \frac{\rho_s[1,j] * \nu_s[1,j] * Sh}{Sc[1,j] * 2H_s}$$

iii. Mass fraction

$$P_{sat}[1,j] = \mathbf{p\_sat}(\mathbf{Water}, T = T_{wall}[1,j])$$

$$x_{f_{wall}}[1,j] = \frac{P_{sat}[1,j]}{P_{atm}}$$

$$m_{f_{wall}}[1,j] = \frac{x_{f_{wall}}[1,j] * m_{water}}{x_{f_{wall}}[1,j] * m_{water} + (1 - x_{f_{wall}}[1,j]) * m_{air}}$$

$$\begin{aligned}
m_f[2,j] &= \frac{\omega_s[2,j]}{\omega_s[2,j] + 1} \\
m_{f_{avg}}[1,j] &= \frac{m_f[1,j] + m_f[2,j]}{2} \\
\frac{\dot{m}_{s_{bottomch}}}{2} (m_f[2,j] - m_f[1,j]) \\
&= g_{m_{water}}[1,j] * (m_{f_{wall}}[1,j] - m_{f_{avg}}[1,j]) \\
&* \frac{2 * A_{plate_{secondhalf}}}{N}
\end{aligned}$$

iv. Top channel energy balance

$$\text{Call ductflow} \left( \begin{array}{l} \text{AirH2O}, T_{p_{avg}}[1,j], P_{ins}, \dot{m}_{top}[1,j], H_p, W_{topch}, \frac{l_{fp}}{2}, \\ \text{RelRough}_p: htc_{T_{top}}[1,j], htc_{H_{top}}[1,j], \Delta P_{top}[1,j], \\ \text{Nusselt}_{top}[1,j], f_{top}[1,j], Re_{top}[1,j] \end{array} \right),$$

$$htc_{top}[1,j] = \frac{htc_{T_{top}}[1,j] + htc_{H_{top}}[1,j]}{2}$$

$$h_p[1,j + 1] = \text{enthalpy}(\text{AirH2O}, T = T_p[1,j + 1], \omega = \omega_s[1,j], P = P_{ins})$$

$$Q_p[1,j] = htc_{top}[1,j] * (T_{p_{avg}}[1,j] - T_w[1,j]) * \frac{2 * A_{plate_{secondhalf}}}{N}$$

$$Q_p[1,j] = \frac{\dot{m}_{top}[1,j]}{2} * h_p[1,j] - \frac{\dot{m}_{top}[1,j + 1]}{2} * h_p[1,j + 1] - \frac{\dot{m}_{s_{bottomch}}}{2} * h_s[1,j]$$

v. Wet channel energy balance

$$T_{s_{avg}}[1,j] = \frac{T_s[1,j] + T_s[2,j]}{2}$$

$$h_s[2,j] = \text{enthalpy}(\text{AirH2O}, T = T_s[2,j], \omega = \omega_s[2,j], P = P_{ins})$$

$$Q_p[1,j] = \frac{\dot{m}_{s_{bottomch}}}{2} * (h_s[2,j] - h_s[1,j])$$

$$Q_s[1,j] = \frac{htc_s}{2} * (T_w[1,j] - T_{s_{avg}}[1,j]) * \frac{2 * A_{plate_{secondhalf}}}{N}$$

$$Q_l[1,j] = g_{m_{water}}[1,j] * (m_{f_{wall}}[1,j] - m_{f_{avg}}[1,j]) * \Delta h_{vap}[1,j] * \frac{2 * A_{plate_{firsthalf}}}{N}$$

$$Q_p[1,j] = Q_l[1,j] + Q_s[1,j]$$

$$\Delta h_{vap}[1,j] = \text{enthalpy\_vaporization}(\text{Water}, T = T_{wall}[1,j])$$

J. Outlet temperatures, humidity ratio and effectiveness calculations

$$\begin{aligned}
 T_{avg} &= \frac{T_{in_p} + T_{in_s}}{2} \\
 T_{op_{avg}} &= \frac{\mathbf{sum}(T_p[i, N + 1], i = 2, M)}{M - 1} \\
 T_{os_{avg}} &= \frac{\mathbf{sum}(T_s[M + 1, j], j = 1, N)}{N} \\
 T_{op_{avg}(C)} &= \mathbf{converttemp}('K', 'C', T_{op_{avg}}) \\
 T_{os_{avg}(C)} &= \mathbf{converttemp}('K', 'C', T_{os_{avg}}) \\
 \omega_{s_{out_{avg}}} &= \frac{\mathbf{sum}(\omega_s[M + 1, j], j = 1, N)}{N} \\
 \Delta h_{vap_{water}} &= \mathbf{enthalpy\_vaporization}(\mathbf{Water}, T = T_{in_p}) \\
 \omega_{p_{out}} &= \omega_{p_{in}} \\
 \dot{m}_{min} &= \mathbf{min}(\dot{m}_{in_{pch}}, \dot{m}_{s_{bottom_{ch}}}) \\
 \varepsilon_{total} &= \frac{\left( \dot{m}_{in_{pch}} * c_{p_{in_p}} * (T_{in_p} - T_{op_{avg}}) \right)}{\dot{m}_{in_{pch}} * \Delta h_{vap_{water}} * (\omega_{in_p} - \omega_{out_p})} \\
 &\quad - \frac{\dot{m}_{min} * c_{p_{in_p}} * (T_{in_p} - T_{in_s}) + \dot{m}_{min} * \Delta h_{vap_{water}} * (\omega_{in_p} - \omega_{in_s})}{\dot{m}_{in_{pch}} * \Delta h_{vap_{water}} * (\omega_{in_p} - \omega_{out_p})} \\
 \varepsilon_{dp} &= \frac{T_{in_p} - T_{op_{avg}}}{T_{in_p} - T_{in_s dp}} \\
 \varepsilon_{wb} &= \frac{T_{in_p} - T_{op_{avg}}}{T_{in_p} - T_{in_s wb}}
 \end{aligned}$$